Lithos 208–209 (2014) 378–392

Contents lists available at ScienceDirect

Lithos

journal homepage: www.elsevier.com/locate/lithos

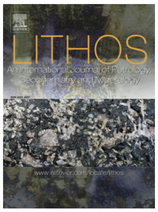

Origin of garnet in aplite and pegmatite from Khajeh Morad in northeastern Iran: A major, trace element, and oxygen isotope approach

Ramin Samadi [a],*, Nathan R. Miller [b], Hassan Mirnejad [c], Chris Harris [d], Hiroshi Kawabata [e], Nargess Shirdashtzadeh [f]

[a] Department of Geology, Science and Research Branch, Islamic Azad University, Tehran, Iran
[b] Department of Geological Sciences, University of Texas at Austin, Austin, TX 78712, USA
[c] Department of Geology, Faculty of Science, University of Tehran, Tehran, Iran
[d] Department of Geological Sciences, University of Cape Town, Rondebosch 7701, South Africa
[e] Research and Education Faculty, Kochi University, Kochi 780-8520, Japan
[f] Department of Geology, Faculty of Science, University of Isfahan, Isfahan, Iran

ARTICLE INFO

Article history:
Received 7 April 2014
Accepted 30 August 2014
Available online 16 September 2014

Keywords:
Garnet
Aplite
Pegmatite
LA-ICP-MS
IRMS
Iran

ABSTRACT

Triassic monzogranites and granodiorites of the Khajeh Morad region in northeastern Iran are cut by two types of garnet-bearing intrusive veins: (1) aplite and (2) granitic pegmatite. The former is composed of quartz, feldspar, muscovite, with minor garnet, biotite, and ilmenite. The latter contains quartz, plagioclase (±quartz and muscovite inclusions), alkali feldspar, and muscovite, with minor amounts of garnet, tourmaline, beryl, columbite, and ilmenite. Garnet in both rock types has MnO > 12 wt.% and CaO < ~2 wt.% with spessartine-rich cores, and a core-to-rim increase in Fe, Mg, and Ca. Garnet cores are enriched in Y, REE, Zr, Nb, Ta, Hf, and U. The Y, HREE, and Mn concentrations show strong positive correlations in both types of garnet associations and decrease from core-to-rim. These core-to-rim elemental variations can be explained by increasing fluid content and H_2O activity in magma, together with decreasing Mn contents of an evolved host melt. Aplite and pegmatite garnet $\delta^{18}O$ values are nearly identical (~10.3‰, $n = 7$, SD = 0.09) and are similar to magmatic garnets in granitoids elsewhere. On the basis of calculated $\delta^{18}O$ values for magma (~12.5 and 12.6‰) and quartz (~13.6‰, $n = 7$, SD = 0.08) as well as the major and trace element characteristics, we suggest that the Khajeh Morad garnets crystallized from a variably fractionated S-type monzogranitic magma.

1. Introduction

Garnet is a common accessory mineral in metamorphic rocks and less frequent in igneous rocks (e.g. London, 2008; Muller et al., 2012). It is potentially useful for magmatic studies because of slow diffusion rates for cations and anions, and resistance to alteration. Compositional zonation in garnet may preserve the compositional changes and temperature–time histories of the magma in which they grew. However, few data are available from garnet in aplite and pegmatite (e.g. Arredondo et al., 2001; Baldwin and Von Knorring, 1983; Gadas et al., 2013; Manning, 1983; Whitworth, 1992), which are generally regarded as having magmatic origins (e.g. Deer et al., 1992; Leake, 1967; Manning, 1983). Thomas and Davidson (2012) suggested that granite and pegmatite melts differ significantly with regard to the dissolved H_2O content in the magma and viscosity at comparable temperatures and pressures, with pegmatite formation involving low viscosity, melt-fluid immiscibility, and extremely evolved melts. Although garnets of granitoids and granitic pegmatites are commonly Fe^{2+}-rich, garnet in granitic aplite and pegmatite commonly has higher Mn and lower Ca contents (e.g. Baldwin and Von Knorring, 1983; London, 2008; Macleod, 1992; Manning, 1983); although Gadas et al. (2013) reported grossular garnet in a leucotonalitic pegmatite. Mn, Fe^{2+} and Ca concentrations in garnet can be used to interpret the origin of this mineral (e.g. Harangi et al., 2001; Samadi et al., 2014b and references therein). For example, garnet xenocrysts in granitoids and metapelites typically exhibit normal zoning, with Mn-rich and Fe-poor cores and core-to-rim decrease of Mn whereas phenocrysts and magmatic garnet in plutonic rocks tend to show reversed zoning with core-to-rim increase of Mn, with increasing differentiation in a melt (e.g. Abbott, 1981a, 1981b; Allan and Clarke, 1981; Day et al., 1992; Green and Ringwood, 1968; Harangi et al., 2001; Harris and Vogeli, 2010; Kawabata and Takafuji, 2005; Koepke et al., 2003; Lackey et al., 2008, 2011, 2012; Leake, 1967; Miller and Stoddard, 1981a, 1981b; Mirnejad et al., 2008; Patranabis-Deb et al., 2008; Samadi et al., 2014b; Schwandt et al., 1996; Spear and Kohn, 1996; Vielzeuf et al., 2005). In contrast, garnets within zoned pegmatite bodies are often characterized by Mn-rich cores and Fe^{2+}-rich rims (Arredondo et al., 2001; Baldwin and Von Knorring, 1983; Manning, 1983; Whitworth, 1992). Knowledge of trace element zoning patterns in garnet is useful for characterizing the

---

* Corresponding author. Tel.: +98 912 4729104.
E-mail address: rsamadi@hotmail.com (R. Samadi).

http://dx.doi.org/10.1016/j.lithos.2014.08.023
0024-4937/© 2014 Elsevier B.V. All rights reserved.

origin of garnet and its host rock. Although trace element zoning of garnets in granitoids, skarns, pelitic and ultramafic rocks is well studied (e.g. Čopjaková et al., 2005; Heimann et al., 2011; Irving and Frey, 1978; Koepke et al., 2003; Lackey et al., 2011; Schwandt et al., 1996; Smith et al., 2004), garnets in granitic pegmatites and aplites have received much less attention (e.g. Gadas et al., 2013; Muller et al., 2012). Trace element zoning in garnets arises from the partitioning of incompatible trace elements into the garnet (relative to more compatible major elements) that accompanies changes in composition of melt, temperature and pressure (e.g. Schwandt et al., 1996 and references therein). The oxygen isotope composition of garnet is a potential useful tracer of the parent magma (Lackey et al., 2006, 2008) because garnet has a high closure temperature to oxygen diffusion (e.g. Farquhar et al., 1996) and does not change its δ^{18}O value once crystallized (e.g. Harris and Vogeli, 2010).

Numerous garnet-bearing aplite and pegmatite veins cut across the Triassic monzogranite–granodiorite bodies in the Khajeh Morad area, in southeastern Mashhad city (Fig. 1). To understand the origin of these garnets, and how they may relate to the time–composition and temperature histories of the rocks in which they grew, we employed LA-ICP-MS, EPMA, and IRMS to establish major and trace element zoning patterns and oxygen isotope compositions of garnet grains from these aplite and pegmatite associations. We then compare Khajeh Morad garnet from aplite–pegmatite associations with similar garnet associations studied elsewhere around the world in order to further understand the origin and petrogenetic implications of garnets. Abbreviations of minerals were adopted from Kretz (1983) and Whitney and Evans (2010).

2. Geological background

Iran is located in the middle of the Alpine-Himalayan orogenic system. The latter forms a continuous suture zone from the eastern Mediterranean area to the northwest Himalayan belt. The study area, located in southeastern Mashhad city, northeastern Iran, forms the eastern portion of a northwest-southeast trending granitoid batholith within the Paleo-Tethys suture zone (Fig. 1). This suture zone includes meta-ophiolites and meta-flysch sequences, representing Paleo-Tethys Ocean closure in the Jurassic period (Alavi, 1991). The meta-ophiolites, meta-flysch and granites are surrounded by metamorphosed marginal continental sediments, consisting of well-layered slate, phyllite, schist, hornfels, marble, quartzite, and skarn (Samadi et al., 2012). Silurian opening of the Paleo-Tethys in northern Iran was followed by its northward subduction beneath the Kopeh Dagh zone (Turan Plate in the southern part of Laurasia) in the Late Devonian, culminating in late Triassic collision between the Iranian Microcontinent and Turan Plate (Alavi, 1991; Natalin and Sengor, 2005). Emplacement of the Mashhad granitoid batholith occurred during the final stages of Paleo-Tethys subduction and early stages of Turan–Iran Plate collision (Mirnejad et al., 2013; Samadi et al., 2014a). The Mashhad batholith consists of granodiorite, monzogranite, and diorite–tonalite–granodiorite suites that were intruded into the metamorphic complex.

In the Khajeh Morad area, granodiorite and monzogranite bodies are cut by aplite and pegmatite veins (Fig. 1). The granodiorites are largely quartz, feldspar, and biotite, whereas monzogranite intrusives contain quartz, feldspar, muscovite, and lesser amounts of biotite. Mirnejad et al. (2013) reported that granodiorite and monzogranite intrusions of Mashhad batholith were emplaced at 212 ± 5.2 Ma and 199.8 ± 3.7 Ma, respectively. Aplite veins were emplaced first, as they are cross-cut by pegmatite veins (Fig. 2). Pegmatite veins consist of quartz, plagioclase, K-feldspar, muscovite, garnet, tourmaline, beryl, columbite, and opaque minerals. The finer grained aplite veins consist of quartz, plagioclase, muscovite, garnet, biotite, and opaque minerals.

3. Analytical techniques

Samples were selected from Khajeh Morad aplite and pegmatites veins for petrographic studies. The garnet grains sampled were sufficiently representative to ascertain geochemical zoning trends within the respective vein associations. Major oxide analyses of core and rim of garnets were carried out by wavelength dispersive electron probe microanalysis (EPMA), using a JEOL JXA-8800 at the Japan Agency for

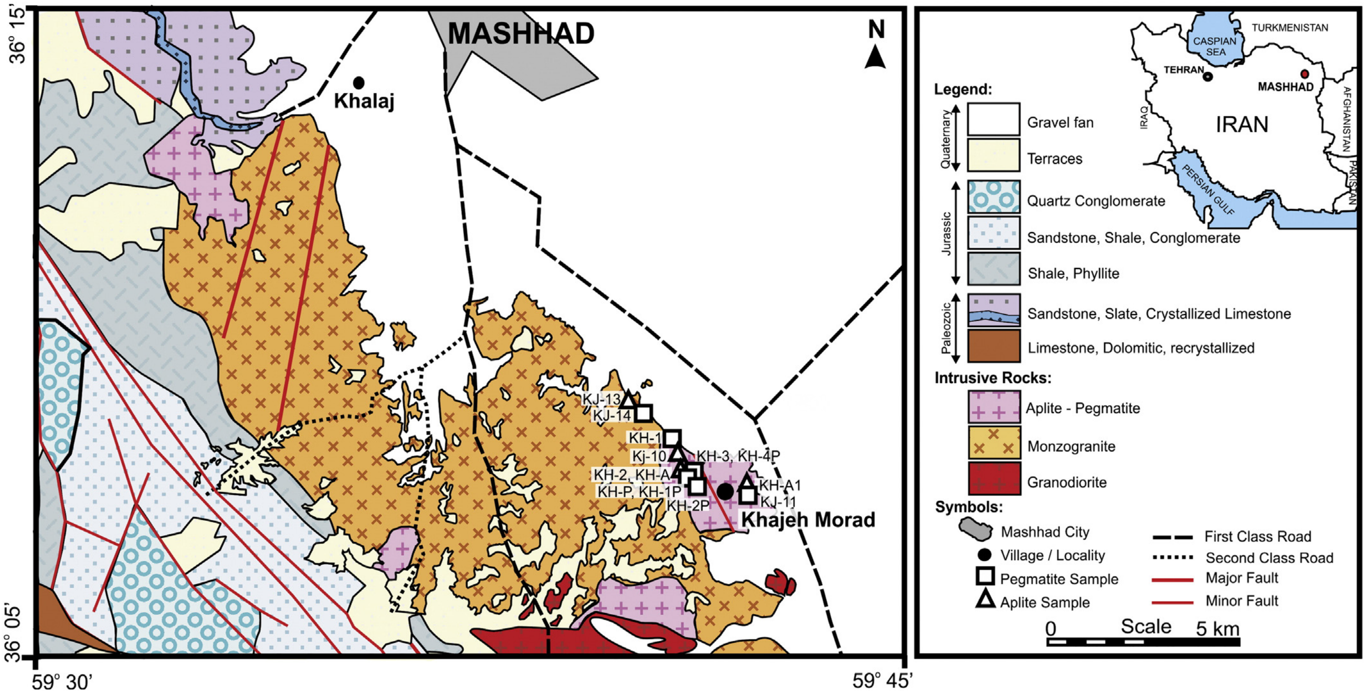

Fig. 1. Geological map of Khajeh Morad in southeastern Mashhad, northeastern Iran (modified after Samadi, 2014) (for interpretation of the references to color in this figure legend, the reader is referred to the web version of the article).

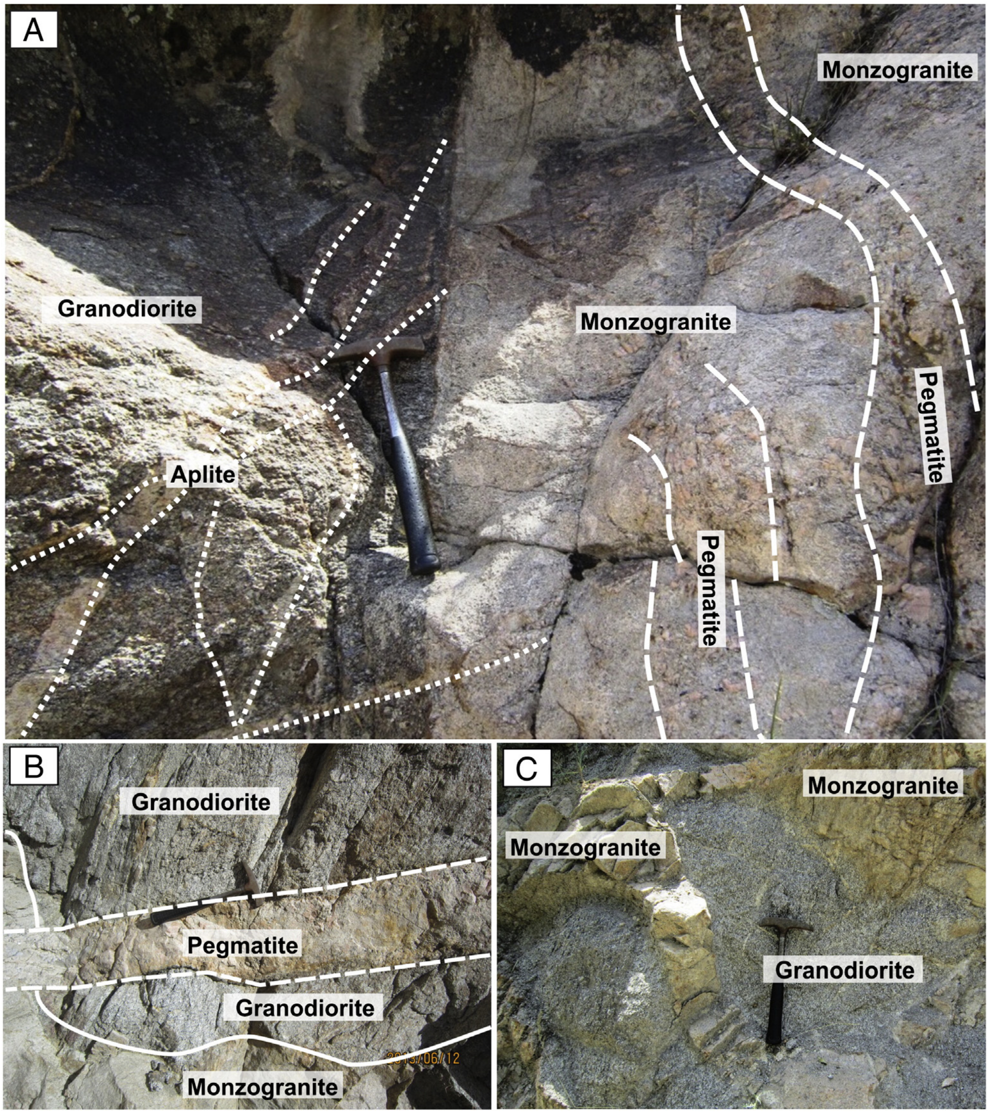

Fig. 2. Field photographs of Khajeh Morad aplite and pegmatite contact relationships. (A) Monzogranite and granodiorite contact, with cutting across aplite (stippled lines) – pegmatite (dashed lines) veins. (B) View of a prominent pegmatite vein cutting across granodiorite and monzogranite. (C) View of weathering-resistant monzogranite veins cutting across the granodiorite.

Marine-Earth Science and Technology (JAMSTEC) and a JEOL Superprobe at the University of Cape Town, South Africa. Operating conditions for both instruments were 15 kV accelerating voltage and 15 nA beam current. Natural and synthetic minerals of known composition were used as standards. Conventional ZAF data corrections were performed for the EPMA data. The representative data are presented in Tables 1 and 2.

Based on petrographic investigations from polished thin sections, several representative garnet grains (9 from aplite, 12 from pegmatite) were selected for in situ trace element analyses, using laser ablation inductively coupled plasma mass spectrometry (LA-ICP-MS). LA-ICP-MS was performed at the University of Texas at Austin using a New Wave UP193-fx (193 nm, 4–6 ns pulse width) excimer laser coupled with an Agilent 7500ce ICP-MS. Laser ablation parameters were determined based upon tests of Khajeh Morad garnets. A large (100 μm) spot was selected to optimize sensitivity and also enable multi-spot transects across individual garnet grains. Laser power, repetition rate, and He-flow were iteratively modulated to obtain the most stable settings over 60-second dwell times. The best settings were determined to be 60% laser power, 10 Hz repetition rate, and a He-flow of 250 mL/min. The 60% laser power setting corresponds to an average fluence of ~7.66 J/cm^2. Pulse-to-pulse laser power variation was maintained within 3.29% of this value during analysis. All samples were preablated for two seconds using a 150 μm spot, 20% laser power, and 10 Hz repetition rate. The quadrupole method involved measurement of 29 analytes, using integration times of 10 ms (^{23}Na, ^{47}Ti, ^{85}Rb, ^{90}Zr), 20 ms (^{7}Li, ^{88}Sr, ^{89}Y, ^{93}Nb, ^{137}Ba, ^{178}Hf, ^{181}Ta, ^{208}Pb, ^{232}Th, ^{238}U), 25 ms (^{139}La, ^{140}Ce, ^{141}Pr, ^{146}Nd, ^{147}Sm, ^{157}Gd, ^{159} Tb, ^{163}Dy, ^{165}Ho, ^{166}Er, ^{169}Tm, ^{172}Yb) and 30 ms (^{153}Eu, ^{175}Lu). A gas blank interval of 45 s was used between all laser measurements to establish baseline sensitivities. Garnet analyses were bracketed hourly by triplicate analyses of laser ablation standards NIST-612, NIST-610, and USGS BCR-2G. Elemental concentrations were derived using Iolite software (Hellstrom et al., 2008), with ^{29}Si as the internal standard. Calibration standards used for garnet analytes (based on similarity of measured concentrations) were as follows: NIST-612 for Li, Rb, Sr, Zr, Ba, Ce, Dy, Ho, Er, Tm, Yb, and Lu; BCR-2G for Na, Nb, La, Pr, Nd, Sm, Eu, Gd, Tb, Hf, Ta, Pb, Th, and U; and NIST-610 for Ti and Y. Recoveries on secondary standards (those not used as the primary calibration standard) among all analytes were typically within 2% of GeoReM (georem.mpch-mainz.gwdg.de) preferred values, with standard deviations better than 13%. Signal among analytes measured in garnets ($n = 53$), as estimated from the ratio of median concentration to the average detection

Table 1
Representative microprobe data (in wt.%) of coarse garnet grains in the aplitic veins and their calculated structural formula based on 12 oxygen atoms. Samples KJ-13 are from the margin zones of aplitic veins whereas samples KJ-10 are picked from the middle zones.

Margin zone of the vein									Middle zone of the vein									
	KJ-13-gr1c	KJ-13-gr1r	KJ-13-gr2c	KJ-13-gr2r	KJ-13-gr4c	KJ-13-gr4r	KJ-13-gr5c	KJ-13-gr5r	KJ-10-gr1c	KJ-10-gr1r	KJ-10-gr2c	KJ-10-gr2r	KJ-10-gr3c	KJ-10-gr3r	KJ-10-gr4c	KJ-10-gr4r	KJ-10-gr5c	KJ-10-gr5r
Sample no.	121	122	124	125	126	127	37	39	82	83	84	85	86	87	88	89	18	20
SiO_2	35.67	36.42	35.83	35.85	36.53	36.58	36.90	36.57	35.99	36.80	36.50	36.71	36.76	36.36	36.54	36.47	37.19	37.20
TiO_2	0.02	0.02	0.06	0.00	0.04	0.00	0.02	0.00	0.06	0.05	0.06	0.00	0.07	0.02	0.04	0.04	0.05	0.02
Al_2O_3	20.09	20.74	20.67	21.07	20.98	20.72	21.55	21.35	20.72	20.63	20.74	20.82	20.85	21.19	21.24	20.92	21.91	21.74
Cr_2O_3	0.00	0.00	0.00	0.00	0.01	0.00	0.00	0.00	0.00	0.00	0.00	0.00	0.00	0.00	0.00	0.02	0.00	0.00
FeO	27.99	29.11	29.17	29.78	28.19	29.16	26.85	29.36	25.60	27.19	26.69	27.36	28.21	27.88	27.36	27.67	26.62	26.90
MnO	13.70	12.63	12.28	11.85	13.38	12.52	13.75	11.67	16.07	13.44	15.50	13.70	14.07	13.15	14.24	12.79	14.77	13.36
MgO	0.28	0.28	0.28	0.27	0.31	0.27	0.26	0.28	0.30	0.65	0.46	0.57	0.57	0.75	0.65	0.76	0.39	0.68
CaO	0.54	0.56	0.60	0.55	0.71	0.59	0.77	0.64	0.54	0.96	0.56	0.84	0.60	0.86	0.75	0.94	0.75	0.91
Na_2O	0.00	0.01	0.00	0.03	0.03	0.00	0.06	0.06	0.00	0.01	0.00	0.00	0.02	0.02	0.00	0.00	0.04	0.00
K_2O	0.01	0.00	0.00	0.00	0.00	0.01	0.00	0.00	0.01	0.00	0.00	0.00	0.01	0.00	0.00	0.00	0.00	0.00
Total	98.28	99.76	98.90	99.39	100.18	99.87	100.15	99.93	99.29	99.72	100.51	100.01	101.15	100.23	100.82	99.60	101.71	100.82
Si	2.99	3.00	2.98	2.96	2.99	3.01	2.99	2.98	2.98	3.01	2.99	3.00	2.99	2.97	2.97	2.99	2.97	2.98
Al^{iv}	0.01	0.00	0.02	0.04	0.01	0.00	0.01	0.02	0.02	0.00	0.01	0.00	0.01	0.03	0.03	0.01	0.03	0.02
Al^{vi}	1.98	2.01	2.01	2.02	2.02	2.01	2.06	2.04	2.01	1.99	1.99	2.01	1.99	2.01	2.01	2.01	2.05	2.05
Ti	0.00	0.00	0.00	0.00	0.00	0.00	0.00	0.00	0.00	0.00	0.00	0.00	0.00	0.00	0.00	0.00	0.00	0.00
Cr	0.00	0.00	0.00	0.00	0.00	0.00	0.00	0.00	0.00	0.00	0.00	0.00	0.00	0.00	0.00	0.00	0.00	0.00
Fe^{3+}	0.01	0.00	0.00	0.00	0.00	0.00	0.00	0.00	0.00	0.00	0.00	0.00	0.01	0.00	0.00	0.00	0.00	0.00
Fe^{2+}	1.95	2.02	2.04	2.08	1.95	2.02	1.90	2.06	1.79	1.88	1.82	1.89	1.91	1.92	1.88	1.92	1.84	1.88
Mn	0.97	0.88	0.86	0.83	0.93	0.87	0.94	0.81	1.13	0.93	1.08	0.95	0.97	0.91	0.98	0.89	1.00	0.91
Mg	0.03	0.03	0.03	0.03	0.04	0.03	0.03	0.03	0.04	0.08	0.06	0.07	0.07	0.09	0.08	0.09	0.05	0.08
Ca	0.05	0.05	0.05	0.05	0.06	0.05	0.07	0.06	0.05	0.08	0.05	0.07	0.05	0.08	0.07	0.08	0.06	0.08
Total	8.01	8.00	8.01	8.02	8.00	7.99	8.00	8.00	8.01	7.99	8.00	8.00	8.00	8.01	8.01	8.00	8.00	8.00
alm	64.68	67.70	68.00	69.26	65.54	67.88	64.56	69.70	59.35	63.16	60.50	63.36	63.51	63.78	62.15	64.39	62.44	63.73
sps	32.53	29.48	29.03	27.99	31.09	29.24	32.11	27.26	37.82	31.35	35.97	31.82	32.42	30.63	33.01	29.76	33.83	30.84
prp	1.16	1.15	1.17	1.11	1.28	1.13	1.06	1.17	1.23	2.66	1.88	2.33	2.32	3.06	2.64	3.10	1.57	2.78
grs	0.90	1.67	1.80	1.63	2.06	1.75	2.27	1.88	1.61	2.83	1.44	2.48	1.47	2.53	2.20	2.70	2.16	2.66
adr	0.74	0.00	0.00	0.00	0.00	0.00	0.00	0.00	0.00	0.00	0.20	0.00	0.28	0.00	0.00	0.00	0.00	0.00
uv	0.00	0.00	0.00	0.00	0.02	0.00	0.00	0.00	0.00	0.00	0.00	0.00	0.00	0.00	0.00	0.05	0.00	0.00

limit, was lowest (<10) for Na, Rb, Sr, Ba, LREE's (La-Ce-Pr-Nd), Pb, and Th; essentially no Ba, La, or Th was detected. All others were substantially higher. LA-ICP-MS data are presented in Tables 3 and 4.

Oxygen isotope analyses were made at the University of Cape Town (UCT). Mineral separates of garnet and quartz were obtained by disaggregating vein samples in a stainless steel percussion mortar. The cleanest and most inclusion-free grains (2 quartz and 2 garnet grains from aplite, 5 quartz and 5 garnet grains from pegmatite) were selected by handpicking under a binocular microscope for analysis. After ultrasonically cleaning (in water and ethanol) and drying, oxygen was extracted from grains using the laser fluorination method of Harris and Vogeli (2010). Each sample was reacted in the presence of approximately 10 kPa of BrF_5, and the purified O_2 collected onto a 5 Å molecular sieve contained in a glass storage bottle. Isotope ratios were then measured off-line using a Finnigan Delta XP mass spectrometer in dual-inlet mode. The estimated precision of $\delta^{18}O$ measurements is 0.14‰ (2σ) for the laser data, based on multiple duplicate analyses ($n = 61$) of the internal MON GT (garnet) standard during the course of this work (2012/2013). A single bulk rock schist sample was also analyzed using conventional methods described in Harris and Ashwal (2002).

4. Results

4.1. Petrography and sample description

Aplite veins in Khajeh Morad granitoids are fine-grained and show granular to micrographic and myrmekitic textures. Veins are mainly 0.1 to 10 cm in width and composed of anhedral to euhedral quartz with undulose extinction, feldspar (albite and microcline, mostly replaced by sericite and clay minerals), muscovite, minor euhedral to subhedral garnet, opaque minerals (mainly ilmenite) and infrequently biotite crystals. Garnets in aplite veins occur mostly as single, isolated euhedral to equidimensional anhedral, inclusion-free, grains (~0.5–1 mm in size), but also as aggregates or "bead strings" of finer grains (~0.1 mm in size, Fig. 3A). According to Macleod (1992), such "beads-on-a-string" texture in some small garnets may be related to the magnetic attraction of the small garnets during formation in a melt due to their iron content, particularly in crystal rims.

Granitic pegmatites in Khajeh Morad occur mainly as veins (ranging from centimeters to meters in width) that cut across aplite veins and monzogranite–granodiorite bodies. The pegmatite veins are characterized by coarse grains that decrease in size outward from vein interiors (≤10 cm) to the outer contact (~2 mm) with the host rock. In general, pegmatite veins consist of coarse-grained (euhedral to xenomorphic) quartz with undulose extinction, sericitized albite plagioclase (± quartz and muscovite inclusions), perthitic K-feldspar (albite and microcline), muscovite, and minor amounts of garnet, tourmaline, beryl, and opaque minerals (ilmenite). Graphic textures are common. Garnet near vein margins occurs as euhedral to anhedral, inclusion-free, grains, which may be coarse (1–2 mm) or fine (~0.2 mm) in size (Fig. 3B).

4.2. Garnet compositions

Chemical compositions and formulae for garnet grains in Khajeh Morad aplite and pegmatite veins are reported in Tables 1 and 2. Sampling was limited to coarse (<0.5 mm) garnets from central and marginal zones of veins. Garnet compositions are predominantly almandine–spessartine, with the pyrope–grossular component (prp + grs) less than 5 mole%, negligible andradite (adr), and uvarovite (uv). Garnets from aplite are higher in alm and grs and lower in sps and prp contents, with the following ranges: alm (63.06–64.85%), sps (33.27–30.23%), prp (1.63–2.54%) grs (1.94–2.36%), adr (0.09–0.00%), and uv (0.00–0.02%) (Table 1). Pegmatite garnets consist of alm (55.92–63.57%), sps (40.29–32.23%), prp (2.40–2.86%), grs (0.94–1.25%), adr (0.44–0.07%), and uv

Table 2
Representative microprobe data (in wt.%) of coarse garnet grains in the pegmatite veins and their calculated structural formula based on 12 oxygen atoms. Samples KJ-11 are from the margin zones of pegmatite whereas samples KJ-14 are picked from the middle zones.

Margin zone of the vein											Middle zone of the vein									
	KJ-11-gr1c	KJ-11-gr1r	KJ-11-gr2c	KJ-11-gr2r	KJ-11-gr3c	KJ-11-gr3r	KJ-11-gr4c	KJ-11-gr4r	KJ-11-gr5c	KJ-11-gr5r	KJ-14-gr1c	KJ-14-gr1r	KJ-14-gr2c	KJ-14-gr2r	KJ-14-gr3c	KJ-14-gr3r	KJ-14-gr4c	KJ-14-gr4r	KJ-14-gr5c	KJ-14-gr5r
Sample no.	5	6	7	8	9	10	11	12	35	33	266	267	268	269	270	271	272	273	30	31
SiO_2	36.19	36.66	36.38	36.50	36.23	36.31	35.73	35.84	36.05	37.02	35.89	36.21	35.89	36.33	35.83	36.50	35.79	36.27	36.62	36.82
TiO_2	0.00	0.00	0.03	0.04	0.02	0.00	0.04	0.03	0.07	0.00	0.04	0.01	0.06	0.00	0.02	0.01	0.02	0.00	0.04	0.00
Al_2O_3	20.81	20.60	20.75	21.37	20.85	21.09	20.79	21.12	21.79	21.80	20.22	21.18	20.38	20.29	20.02	20.82	20.46	20.82	20.86	21.47
Cr_2O_3	0.00	0.00	0.00	0.00	0.01	0.00	0.00	0.00	0.00	0.00	0.00	0.00	0.00	0.00	0.00	0.00	0.03	0.00	0.00	0.00
FeO	25.17	27.67	25.51	29.18	25.03	28.45	25.25	27.34	24.90	27.63	21.16	26.93	21.33	27.05	21.43	26.66	21.06	27.08	20.94	26.37
MnO	16.50	13.80	14.88	13.21	16.60	13.18	16.18	14.07	16.78	13.91	20.94	14.21	20.81	13.71	20.50	14.01	21.14	14.41	20.77	14.26
MgO	0.55	0.60	0.57	0.51	0.56	0.52	0.52	0.58	0.54	0.55	0.32	0.88	0.37	0.88	0.39	0.84	0.36	0.80	0.39	0.81
CaO	0.46	0.37	0.47	0.37	0.47	0.30	0.43	0.37	0.46	0.35	0.47	0.58	0.45	0.56	0.33	0.56	0.39	0.63	0.42	0.60
Na_2O	0.00	0.04	0.01	0.04	0.02	0.03	0.06	0.06	0.00	0.02	0.01	0.01	0.01	0.02	0.02	0.02	0.01	0.01	0.02	0.00
K_2O	0.01	0.02	0.01	0.00	0.01	0.02	0.02	0.02	0.00	0.00	0.00	0.01	0.00	0.02	0.01	0.00	0.00	0.00	0.00	0.00
Total	99.69	99.76	98.60	101.22	99.80	99.90	99.01	99.43	100.59	101.27	99.03	100.00	99.30	98.85	98.54	99.41	99.26	100.03	100.06	100.33
Si	2.98	3.01	3.00	2.96	2.98	2.98	2.97	2.96	2.93	2.97	2.99	2.96	2.98	3.01	3.00	3.00	2.97	2.98	3.00	2.98
Al^{iv}	0.02	0.00	0.00	0.04	0.02	0.02	0.03	0.04	0.07	0.03	0.01	0.04	0.02	0.00	0.00	0.00	0.03	0.02	0.00	0.02
Al^{vi}	2.01	2.00	2.03	2.01	2.01	2.02	2.01	2.02	2.03	2.05	1.97	2.01	1.98	1.98	1.97	2.02	1.98	2.00	2.01	2.04
Ti	0.00	0.00	0.00	0.00	0.00	0.00	0.00	0.00	0.00	0.00	0.00	0.00	0.00	0.00	0.00	0.00	0.00	0.00	0.00	0.00
Cr	0.00	0.00	0.00	0.00	0.00	0.00	0.00	0.00	0.00	0.00	0.00	0.00	0.00	0.00	0.00	0.00	0.00	0.00	0.00	0.00
Fe^{3+}	0.00	0.00	0.00	0.00	0.00	0.00	0.00	0.00	0.00	0.00	0.02	0.00	0.02	0.00	0.02	0.00	0.01	0.00	0.00	0.00
Fe^{2+}	1.74	1.92	1.81	2.00	1.73	1.98	1.76	1.91	1.73	1.92	1.45	1.86	1.46	1.87	1.48	1.85	1.45	1.86	1.46	1.84
Mn	1.15	0.96	1.04	0.91	1.16	0.92	1.14	0.98	1.16	0.95	1.48	0.99	1.46	0.96	1.45	0.97	1.49	1.00	1.44	0.98
Mg	0.07	0.07	0.07	0.06	0.07	0.06	0.06	0.07	0.07	0.07	0.04	0.11	0.05	0.11	0.05	0.10	0.04	0.10	0.05	0.10
Ca	0.04	0.03	0.04	0.03	0.04	0.03	0.04	0.03	0.04	0.03	0.04	0.05	0.04	0.05	0.03	0.05	0.03	0.06	0.04	0.05
Total	8.01	7.99	7.99	8.02	8.01	8.01	8.01	8.02	8.03	8.01	8.01	8.02	8.01	7.99	8.00	8.00	8.01	8.01	8.00	8.00
alm	57.75	64.24	61.07	66.18	57.51	66.25	58.21	63.23	56.97	64.80	47.86	61.42	47.99	62.36	48.85	62.19	47.29	61.19	48.84	61.97
sps	38.62	32.21	35.19	30.67	38.80	30.75	38.35	33.26	39.43	31.97	49.42	33.23	49.12	32.34	48.57	32.69	50.03	33.64	48.32	32.99
prp	2.27	2.46	2.35	2.08	2.31	2.13	2.15	2.42	2.24	2.21	1.33	3.64	1.53	3.65	1.61	3.46	1.50	3.30	1.61	3.28
grs	1.36	1.09	1.40	1.08	1.35	0.87	1.30	1.10	1.37	1.01	0.37	1.71	0.46	1.49	0.00	1.65	0.33	1.65	1.23	1.75
adr	0.00	0.00	0.00	0.00	0.00	0.00	0.00	0.00	0.00	0.00	1.02	0.00	0.90	0.17	0.97	0.00	0.75	0.21	0.00	0.00
uv	0.00	0.00	0.00	0.00	0.03	0.00	0.00	0.00	0.00	0.00	0.00	0.00	0.00	0.00	0.00	0.01	0.10	0.01	0.00	0.00

Table 3
LA-ICP-MS data (in ppm) of garnet in aplite of Khajeh Morad.

Sample no.	1-Rim1	1-Mid2	1-Mid3	1-Core4	1-Mid5	1-Mid6	1-Rim7	2-1small	2-2small	2-4small	2-5small	2-6small
Li	97	177	188	213	187	136	96	107	104	93	107	128
Na	75	94	143	168	155	107	62	73	86	75	87	81
Ti	222	426	737	594	745	326	229	294	272	264	333	343
Rb	0.18	0.08	0.16	0.08	b.d.	0.08	0.05	b.d.	b.d.	0.10	0.04	b.d.
Sr	0.004	0.01	0.03	0.054	0.026	b.d.	b.d.	0.003	b.d.	b.d.	0.016	b.d.
Y	911	583	1333	1800	1216	694	1004	917	880	819	901	997
Zr	6.7	15.0	30.3	15.4	35.3	12.3	7.7	9.9	7.4	7.2	8.7	10.2
Nb	0.12	3.68	42.65	5.38	49.06	2.51	0.24	1.70	0.63	0.51	0.90	3.26
La	b.d.	b.d.	0.005	b.d.	b.d.	b.d.	b.d.	b.d.	b.d.	b.d.	b.d.	b.d.
Ce	b.d.	0.003	0.038	0.004	0.041	0.016	b.d.	0.058	b.d.	0.008	0.007	b.d.
Pr	b.d.	b.d.	0.021	0.009	0.02	0.013	b.d.	0.019	0.002	b.d.	0.001	0.013
Nd	0.129	0.105	0.404	0.198	0.578	0.251	0.226	0.517	0.264	0.205	0.337	0.278
Sm	1.566	1.195	2.646	2.053	2.788	1.241	1.831	3.214	2.272	2.476	2.882	3.252
Eu	0.083	0.091	0.125	0.179	0.121	0.102	0.118	0.087	0.079	0.083	0.112	0.082
Gd	18.1	12.3	20.6	18.8	21.7	13.3	21.4	21.4	19.0	20.0	24.3	23.6
Tb	12.0	7.9	12.9	13.7	13.3	8.6	14.0	11.5	12.0	11.3	13.2	13.4
Dy	107.3	72.2	130.5	158.2	124.4	79.3	119.0	101.9	100.4	95.9	106.1	113.5
Ho	22.4	14.6	36.5	51.5	32.6	17.5	24.1	22.9	21.2	19.7	21.5	24.3
Er	64.5	41.4	150.7	241.0	127.3	53.5	70.2	79.1	64.6	59.1	66.0	78.8
Tm	10.1	5.8	30.6	57.1	24.6	8.1	10.6	15.0	10.7	9.7	10.5	13.4
Yb	62	32	251	520	187	49	67	113	73	63	72	89
Lu	6.7	3.3	35.4	82.3	25.5	5.4	7.3	14.2	7.8	7.1	7.7	10.7
Hf	0.22	0.96	2.06	0.88	2.44	0.76	0.18	0.41	0.28	0.26	0.33	0.41
Ta	0.08	8.85	23.46	2.98	32.03	6.63	0.23	1.15	0.47	0.46	0.84	1.84
Pb	b.d.	b.d.	b.d.	b.d.	b.d.	b.d.	b.d.	0.04	0.02	0.02	0.04	b.d.
Th	b.d.	b.d.	0.02	b.d.	0.03	0.06	b.d.	0.17	b.d.	b.d.	b.d.	b.d.
U	0.02	0.25	2.09	0.30	2.60	0.65	0.03	1.41	0.07	0.09	0.10	0.21
Eu/Eu*	0.05	0.07	0.05	0.09	0.05	0.08	0.06	0.03	0.04	0.04	0.04	0.03

Note: b.d. = below detection limit; $Eu/Eu^* = Eu_n/(Sm_n \cdot Gd_n)^{0.5}$.

(0.01–0.01%) (Table 2). Individual garnets show Fe increasing, and Mn decreasing, from core-to-rim. Garnet core-to-rim compositions consistently vary in the same way between garnets sampled from middles of veins and garnets sampled progressively outward toward the intrusive contact, with Fe comparatively enriched and Mn comparatively depleted in grains from vein interiors (Tables 1 and 2).

4.3. Trace element compositions of garnet

Trace element data for Khajeh Morad garnets are presented in Tables 3 and 4. Fig. 4 shows analytical spots and spot-traverse locations for small and coarse garnet grains. Only coarse grains show significant compositional variations between the two vein associations (Figs. 5 and 6). In general, aplite and pegmatite garnets are both strongly enriched in heavy rare earth elements (HREE) and extremely depleted in light rare earth elements (LREE, La below detection) relative to chondrite (Figs. 5A, 6A and 6C). Both garnet associations exhibit highly depleted Eu/Eu* values (0.02–0.13) and negligible variations in $(Sm/Yb)_n$ ratio (~0.0047 and 0.0053), with strong positive Ta and negative Sr and Ti anomalies on primitive mantle normalized patterns (Figs. 5B, 6B and 6D). Some differences in trace element composition between the two garnet associations are evident in that aplite garnets exhibit core-to-rim decreases in Y, U, Ta, and Nb, whereas pegmatite garnets exhibit core-to-rim decreases in HREEs.

4.4. Oxygen isotope composition of garnet and quartz

Quartz in Khajeh Morad aplite and pegmatite has $\delta^{18}O$ values of ~13.7‰ ($n = 2$) and ~13.6‰ ($n = 5$), respectively (Table 5), and the coexisting garnet has average $\delta^{18}O$ values of 10.3‰ in both the aplites ($n = 5$) and pegmatites ($n = 2$) (Table 5). The average $\Delta_{\text{quartz–garnet}}$ values of 3.5 and 3.3‰ for aplite and pegmatite veins and assuming equilibrium, represent temperatures of 610 °C and 629 °C, respectively (Table 5), using the fractionation equation of Valley et al. (2003) in which $\Delta_{\text{quartz–garnet}} = 2.71{*}10^6/T^2$. Because garnet has a much higher temperature of closure to diffusion than quartz (e.g. Farquhar et al., 1996), these temperatures are probably lower than the actual melt temperatures because of the likely increase in $\delta^{18}O$ value of the quartz during slow cooling.

5. Discussion

Manning (1983) suggested that garnets in pegmatite show low nucleation density, rapid growth with slow cation diffusion for the crystal and rapid cation diffusion for the pegmatitic liquid, whereas, aplitic garnets are characterized by slow growth and fast cation diffusion for both the crystal and magma. Garnets in late differentiates (aplites and pegmatites) are magmatic in origin, often occurring as relatively Mn-rich solid solutions of almandine–spessartine (Manning, 1983) or rich in spessartine (Whitworth, 1992). Garnet from less fractionated pegmatites, however, is typically Fe-rich (Muller et al., 2012). In the following section, we further consider the origin of garnet based on major and trace element contents, and oxygen isotope composition.

5.1. Major elements of garnet

Aplite–pegmatite garnets have been shown to exhibit quite different compositions and zoning compared to garnets in granitic batholiths and metapelitic rocks (Table 6). For example, granitoids typically contain magmatic garnet crystals that are unzoned in composition (e.g. Aydar and Gourgaud, 2002; Mirnejad et al., 2008; Patranabis-Deb et al., 2008) or have oscillatory compositional zoning (e.g. Day et al., 1992; Kano, 1983; Kawabata and Takafuji, 2005; Samadi, 2009, 2014; Samadi et al., 2014b). Garnets from aplite–pegmatite are often Fe–Mn rich, and exhibit pronounced core-to-rim decrease in Mn (e.g. Baldwin and Von Knorring, 1983; Gadas et al., 2013; Manning, 1983; Thöni et al., 2003; Whitworth, 1992), whereas garnets from granitoids are mostly Fe-rich and exhibit weak core-to-rim increase in Mn (e.g. Allan and Clarke, 1981; Day et al., 1992; Green and Ringwood, 1968; Harangi et al., 2001; Kawabata and Takafuji, 2005; Koepke et al., 2003; Mirnejad et al., 2008; Samadi, 2014; Samadi et al., 2014b; Spear and Kohn, 1996; Vielzeuf et al., 2005; Wang et al., 2003). Other chemical characteristics of magmatic,

Table 4
LA-ICP-MS data (in ppm) of garnet in pegmatite of Khajeh Morad.

Sample no.	5-Rim1	5-Mid2	5-Mid3	5-Mid4	5-Mid5	5-Core6	5-Mid7	5-Mid8	5-Mid9	5-Rim10	4-1small	4-2small	4-3small	4-4small	4-5small	4-6small	4-7small
Li	87	149	73	121	114	163	105	115	95	148	112	99	108	100	128	125	153
Na	64	78	41	99	74	97	76	107	61	56	56	60	95	89	87	79	109
Ti	219	240	321	265	247	404	191	274	408	274	328	240	226	271	325	426	332
Rb	0.11	0.00	b.d.	0.09	b.d.	b.d.	b.d.	0.05	b.d.	0.02	0.09	b.d.	0.03	0.11	0.04	0.05	b.d.
Sr	b.d.	b.d.	b.d.	0.032	b.d.	b.d.	0.016	0.002	b.d.	b.d.	0.007	b.d.	0.046	b.d.	0.02	b.d.	0.004
Y	586	1515	282	1371	606	1135	936	1081	468	1775	734	682	1104	925	1191	897	1439
Zr	7.5	10.2	6.6	8.7	9.7	13.3	6.5	8.3	9.7	13.0	13.2	6.7	7.4	10.0	11.1	15.2	13.3
Nb	0.21	0.85	1.16	0.09	0.22	0.74	0.12	0.09	0.08	1.01	2.07	0.71	0.28	7.43	1.76	12.99	2.45
La	b.d.	b.d.	b.d.	b.d.	b.d.	b.d.	b.d.	b.d.	b.d.	b.d.	b.d.	b.d.	0.161	b.d.	b.d.	b.d.	b.d.
Ce	b.d.	b.d.	b.d.	b.d.	b.d.	b.d.	b.d.	b.d.	b.d.	b.d.	0.01	b.d.	0.825	0.01	0.007	0.011	0.003
Pr	b.d.	0.004	0.004	b.d.	b.d.	b.d.	b.d.	b.d.	0.006	0.008	0.008	b.d.	0.144	0.01	0.01	0.013	0.013
Nd	0.2	0.283	0.203	0.275	0.125	0.093	0.088	0.136	0.303	0.292	0.407	0.189	0.716	0.306	0.317	0.532	0.331
Sm	1.994	3.008	2.122	1.605	0.834	1.846	0.885	1.684	2.178	3.226	3.537	2.485	2.726	2.84	3.039	4.196	3.608
Eu	0.11	0.11	0.188	0.188	0.101	0.122	0.135	0.211	0.19	0.135	0.096	0.085	0.099	0.089	0.104	0.08	0.066
Gd	18.6	26.4	16.4	22.5	10.8	19.0	11.4	19.2	20.0	32.8	22.4	20.0	22.0	24.6	24.8	29.3	26.2
Tb	11.0	17.3	7.5	15.0	7.3	13.7	8.7	13.3	10.2	21.3	11.6	10.6	14.1	13.6	14.6	14.4	16.6
Dy	81.7	167.2	45.3	155.2	71.8	131.8	96.6	127.7	69.5	206.3	88.5	83.5	128.9	113.3	132.7	107.7	160.1
Ho	12.6	38.3	6.3	39.6	16.1	30.6	27.0	29.1	10.9	47.5	17.4	15.8	28.0	22.7	30.2	22.5	37.8
Er	28.3	132.8	14.7	137.1	49.0	90.6	100.5	93.5	26.2	160.1	54.6	45.6	89.6	70.6	103.2	77.8	134.4
Tm	3.6	23.6	2.1	23.1	6.9	12.8	17.2	15.0	3.3	28.0	9.2	7.2	14.9	11.0	18.9	15.1	25.9
Yb	20	172	12	153	42	75	116	100	19	199	65	49	104	73	135	118	198
Lu	1.7	20.0	1.4	18.7	5.0	8.7	14.6	11.9	2.0	23.8	7.8	5.5	12.3	8.3	15.8	15.5	25.9
Hf	0.20	0.38	0.17	0.29	0.48	0.52	0.23	0.29	0.24	0.51	0.50	0.18	0.32	0.46	0.40	0.79	0.50
Ta	0.19	0.50	0.29	0.12	1.22	1.17	0.40	0.14	0.19	0.58	1.53	0.57	0.19	3.26	1.17	6.31	1.68
Pb	0.02	b.d.	0.00	b.d.	0.02	0.03	0.02	0.02	0.02	0.02	0.01	0.02	0.03	b.d.	0.01	b.d.	0.01
Th	b.d.	b.d.	b.d.	b.d.	b.d.	b.d.	b.d.	b.d.	b.d.	b.d.	b.d.	b.d.	0.03	0.00	b.d.	0.01	b.d.
U	0.06	0.08	0.03	0.03	0.05	0.05	0.03	0.03	0.02	0.09	0.16	0.06	0.11	0.48	0.12	0.89	0.18
Eu/Eu*	0.06	0.04	0.10	0.10	0.10	0.06	0.13	0.11	0.09	0.04	0.03	0.04	0.04	0.03	0.04	0.02	0.02

Note: b.d. = below detection limit; Eu/Eu* = $Eu_n/(Sm_n \cdot Gd_n)^{0.5}$.

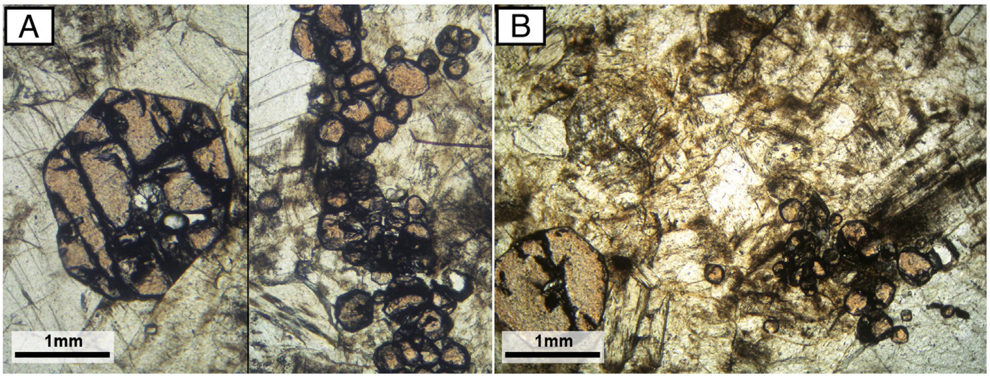

Fig. 3. (A) Coarse and fine, euhedral to spherical, garnet grains from an aplitic vein. Garnets may be solitary or occur as aggregates ("bead of strings"). (B) Coarse and fine, euhedral to anhedral, inclusion-free garnets grains from a sample near the margin of a pegmatite vein.

metapelitic and aplite–pegmatite garnets are compared and summarized in Table 6. In Fig. 7, we compare garnets from Khajeh Morad granitic aplite–pegmatite associations with (1) nearby magmatic garnets of granitoids and metamorphic garnets of metapelitic rocks, and (2) other worldwide examples of magmatic garnets from granitic aplite–pegmatite, in terms of CaO versus MnO composition. This comparison demonstrates that garnets from granitic aplite–pegmatites characteristically have MnO >12 wt.% and CaO <~2 wt.% whereas the garnets of metapelitic rocks and granitoids have lower MnO (~<12 wt.% and ~5 wt.%, respectively) and higher CaO (~0–4 wt.% and ~0–8 wt.%, respectively).

Xenocrystic garnets in igneous rocks are characterized by Mn-normal zoning with core-to-rim depletion in Mn, whereas magmatic garnets exhibit reversed zoning with core-to-rim enrichment in Mn (Allan and Clarke, 1981). Oscillatory compositional zoning is also regarded as a common characteristic of garnet xenocrysts of metamorphic origin in granitoids (e.g. Green and Ringwood, 1968; Harrison, 1988; Manning, 1983). According to Dahlquist et al. (2007), core-to-rim Mn decrease or "Mn bell-shaped profiles" in garnets must be of metamorphic origin (i.e., xenocrystic) or form from silica-rich granitic magmas (SiO_2 = 73–76%) at temperatures below 700 °C. Metamorphic garnets from pelitic protoliths also show Mn-rich and Fe-poor cores (e.g. Schwandt et al., 1996). Garnet formed during prograde metamorphic activity is thought to be normally zoned, with Mn-rich cores and Fe-rich rims (Deer et al., 1982).

Magmatic garnets with Mn-rich cores and Fe-rich rims have been reported from pegmatites of Hub Kapong (Thailand) (Manning, 1983), Cairnsmore of Fleet Granite (Southern Uplands, Scotland) (Macleod, 1992) and Ötztal basement (Tyrol, Eastern Alps) (Thöni and Miller, 2004). Khajeh Morad garnets in aplite and pegmatite vein associations are characterized by Mn-rich cores with core-to-rim increase of Fe, Mg, and Ca. Khajeh Morad pegmatite garnets, however, are more enriched (~4–12 mole% higher) in sps + prp and have lower alm + grs contents (~4–13 mole% lower) than aplites (Tables 3 and 4). This less pronounced compositional zonation of aplite garnet may be attributed to crystallization at lower temperatures, as suggested by Manning (1983). In addition, garnet in Khajeh Morad pegmatite veins has a wider variation in alm and sps components (Δ_{alm} (mole%)$_{\text{rim-core}}$ = 8.4 and Δ_{sps} (mole%)$_{\text{rim-core}}$ =

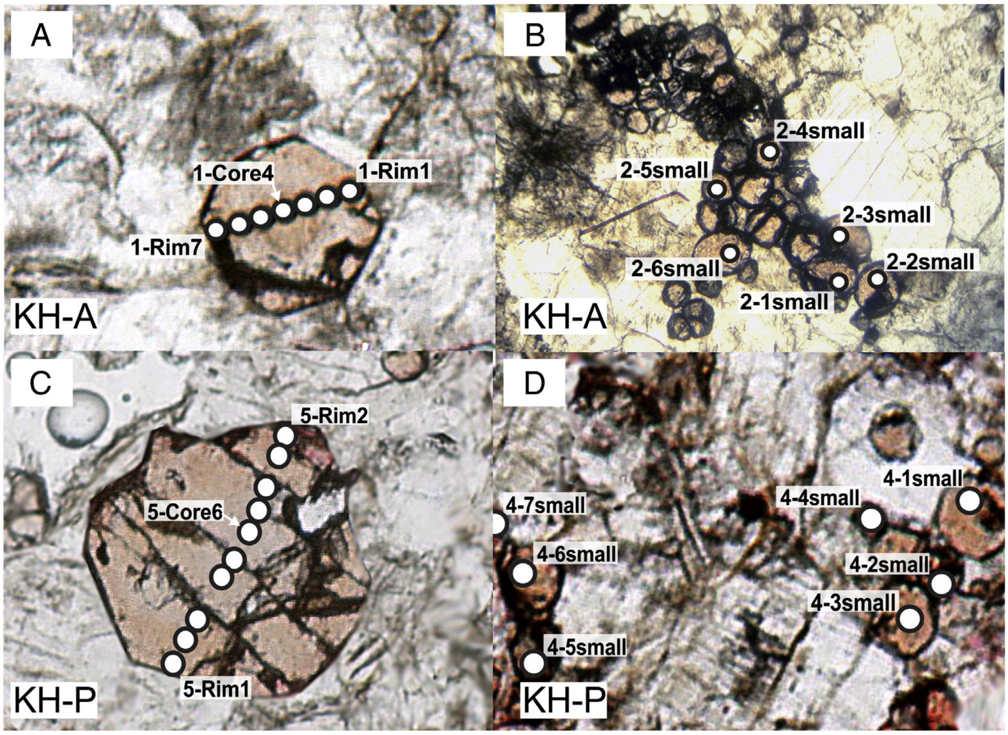

Fig. 4. Locations of laser ablation spots and grain transects on the coarse and fine garnet grains from: (A, B) aplite vein; (C, D) pegmatite vein. Spots diameters are 100 μm.

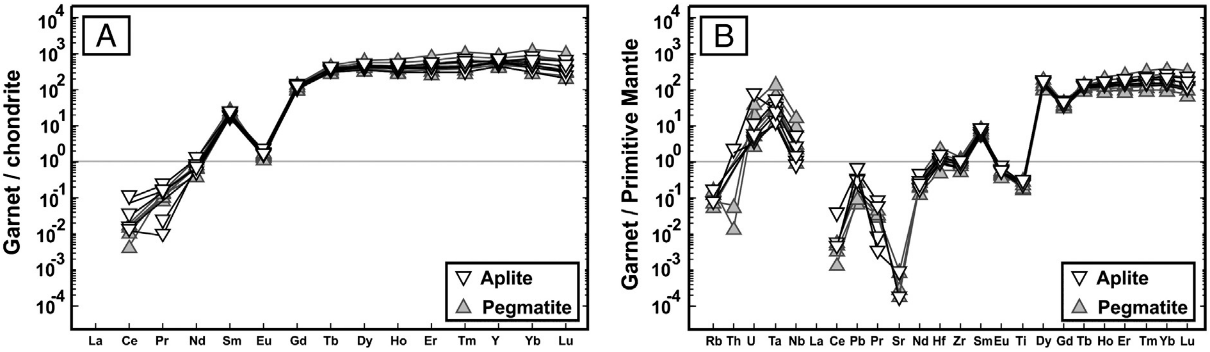

Fig. 5. Composition of small garnet grains in Khajeh Morad aplite and pegmatite on: (A) chondrite normalized diagram of REE and Y; (B) primitive mantle normalized patterns of elements for the small garnet grains in Khajeh Morad aplite and pegmatite. Normalization values are after McDonough and Sun (1995).

−8.9) than garnet in aplite veins (Δ_{alm} (mole%)$_{rim\text{-}core}$ = 1.41 and Δ_{sps} (mole%)$_{rim\text{-}core}$ = −2.74). On an alm versus sps plot (Fig. 8), Khajeh Morad garnet compositions show a linear trend between Mn-rich cores and Fe-rich rims.

Miller and Stoddard (1981a) and Abbott (1981b) argued that the Mn/(Fe + Mg) ratio in magmatic garnet increases with increasing differentiation in a melt, and that Mn-rich garnet probably precipitates from evolved Mn-rich melts. Abbott (1981b) suggested that disappearance of biotite during the final stages of fractional crystallization may lead to garnetiferous aplites and pegmatites. Thus, the melt moves along the liquid–garnet–muscovite cotectic by muscovite crystallization, and consequently higher Fe/Mg and Mn/Fe contents of the melt (Miller and Stoddard, 1981b). In fact, as an indicator of the degree of fractionation of pegmatite-forming melts, MnO/(FeO + MnO) value of garnet crystals increases with increasing fractionation of the melt, controlled by coexisting Mn–Fe-consuming minerals (Muller et al., 2012). Muller et al. (2012) suggested that where Fe-compatible mafic minerals (e.g. biotite, magnetite, allanite, columbite and tourmaline) coexist with garnet, the garnet MnO/(MnO + FeO) values increase core-to-rim, whereas in settings where garnet alone supplies Fe and Mn, the melt becomes depleted in Mn relative to Fe, and garnet MnO/(MnO + FeO) values decrease core-to-rim. Moretz et al. (2013) also showed that garnet from the least evolved melts has the lowest MnO, MgO and CaO, and the highest FeO contents (Fig. 9). Such fractionation of Fe–Mn–(Mg) during crystallization seems evident in the garnet in aplite and pegmatite of Khajeh Morad. For example, MnO and FeO compositions show regular spatial variations both within veins (interiors to wall-proximal exteriors) and within individual crystals (core-to-rim position).

As shown in Fig. 10, the core and rim composition of Khajeh Morad garnet grains are very similar in composition (Fe, Mn) to Fe–Mn garnets of contact zones in Baldwin and Von Knorring (1983) except that garnet cores from middle zones of pegmatite veins mostly have similar composition to Fe–Mn garnets of middle zones of Baldwin and Von Knorring (1983). Khajeh Morad garnets from vein interiors (representing medium-evolved melts last to crystallize) have higher MnO and lower FeO contents compared to garnets from vein rims (representing less-evolved melts first to crystallize; Figs. 9 and 10). Fe^{2+} decreases, and Mn increases from the wall zone to the core zone, are ascribed to increasing H_2O activity (a_{H2O}) in magma during the pegmatite crystallization (Arredondo et al., 2001). Within individual garnet crystals, MgO

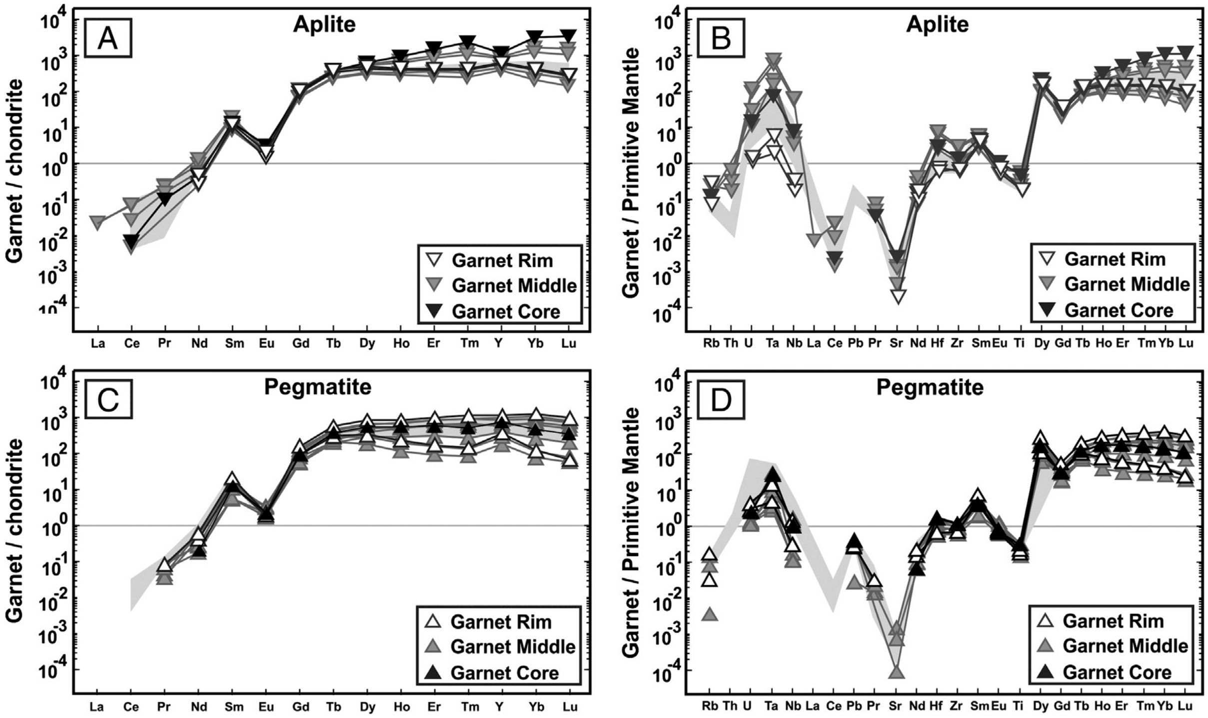

Fig. 6. Chondrite normalized and primitive mantle normalized patterns of elements for rim, middle and the core composition of coarse grain garnets in comparison to fine garnet grains (light gray fields, cf. Fig. 5) in: (A, B) aplite; (C, D) pegmatite. Normalization values are after McDonough and Sun (1995).

Table 5
$\delta^{18}O$ values (in ‰) of garnet and quartz grains from Khajeh Morad aplite and pegmatite veins in comparison with the garnets of mica schists and I-type granitoid from Khalaj (Samadi, 2014) and Dehnow (Samadi et al., 2014b) areas. $\delta^{18}O$ of magma is calculated based on $\Delta_{quartz-magma} = 1.1‰$ of Kontak and Kyser (2009). Oxygen closure temperature is calculated based on Valley et al. (2003).

Rock type	Sample no.	$\delta^{18}O_{garnet}$	$\delta^{18}O_{quartz}$	$\delta^{18}O$ of magma ($\Delta_{quartz-magma} = 1.1‰$)	$\Delta_{quartz-garnet}$	Temperature (°C)
Khajeh Morad pegmatite	KH-1	10.3	13.6	12.5	3.4	626
	KH-3	10.3	13.6	12.5	3.3	633
	KH-1P	10.3	13.6	12.5	3.3	632
	KH-2P	10.3	13.7	12.6	3.3	628
	KH-4P	10.1	13.5	12.4	3.4	623
Khajeh Morad aplite	KH-2	10.2	13.7	12.6	3.5	611
	KH-A1	10.4	13.7	12.6	3.3	638
Dehnow I-type granitoid ($n = 6$)	DH-2011-1*	8.5 (±0.1)	11.9 (±1.5)	10.8	3.3	634
Dehnow Mica schist ($n = 5$)	DH-2011-2*	13.0 (±0.5)	n.a.	–	n.a.	–
Khalaj Mica schist ($n = 1$)	K-2011-2**	12.7	n.a.	–	n.a.	–

Note: *Average data from Samadi et al. (2014b); **data from from Samadi (2014); n.a. = not analyzed.

(and FeO) increases core-to-rim, whereas CaO (and MnO) decreases core-to-rim (Fig. 9). Since the Mn/Fe partition coefficient between garnet and melt is >1, melts should evolve toward lower Mn as magmatic garnets grow (London, 2008). These spatial distributions thus support that Mn-rich garnet in Khajeh Morad aplite and pegmatite relates to the Mn content of the parental magma, since (1) the Mn/(Fe + Mg) ratio can increase with increasing differentiation in a melt (Miller and Stoddard, 1981a), and (2) spessartine-rich magmatic garnet probably precipitates from evolved Mn-rich cooling melts by Rayleigh fractionation (Baldwin and Von Knorring, 1983; Macleod, 1992; Manning, 1983; Thöni and Miller, 2004; Whitworth, 1992).

5.2. Trace element zoning in garnet

According to Spear and Kohn (1996), trace element zoning (i.e. core-to-rim spatial variations within crystals) is least modified by diffusive processes, so patterns of geochemical zonation can be used to interpret the extent of melting and to assess the kinetics of melting and participation of accessory phases in crustal anatexis. ΣREE and Y show positive correlations in the Khajeh Morad garnets of aplite–pegmatite veins. The REEs are enriched in cores of aplitic garnets, but have slightly irregular core-to-rim distributions in pegmatitic garnets (Figs. 11 and 12). High field strength elements (HFSE, such as Zr, Nb, Ta, Hf, and U) have distributions similar to the REE, being more enriched in aplitic garnets than in pegmatitic garnets (Figs. 11 and 12). Ti, Y, and Li are enriched in both garnet associations, but decrease from core-to-rim in aplitic garnets and exhibit oscillatory trends in pegmatitic garnets (Figs. 11 and 12). The oscillatory Y zoning in garnets of pegmatite, ranging from 281 to 1775 ppm, is suggestive of two growth stages, each characterized by core-to-rim decrease in Y and HREE, as similarly observed for aplitic garnets (Fig. 12). Aplitic garnets are characterized by Y-rich cores (>1000 ppm) compared to margins, with smooth decreases toward edges (Fig. 11), similar to core-to-rim Mn zoning. Jaffe (1951) suggested the substitution scheme of Y for Mn (Y^{3+}, Al^{3+} for Mn^{2+}, Si^{4+}) in the manganese garnet (spessartine) due to similar ionic radius. The rimward decrease in Y and REE may be related to the introduction of a new magma with a different REE composition, to magma fractionation (Smeds, 1994), and/or fluid-phase accumulation that was unfavorable for the involvement of REE in the garnet structure (Wang et al., 2003). For pegmatite associations, Muller et al. (2012) suggested that average Y and HREE contents in garnet decrease with increasing magma fractionation and chemical changes in the melt (increasing of MnO) and fluid composition. For Khajeh Morad aplite and pegmatite garnets, we find that Y decreased slightly during growth (i.e. Y decreases towards the rim), similar to observations for garnets from the evolved Solas and Hovasen pegmatites of Norway (Muller et al., 2012).

5.3. Oxygen isotope of garnet and quartz

Oxygen isotopes can be a powerful tool for understanding the genesis of garnet in granitoids and pegmatites, because garnet is resistant to alteration and has a very high closure temperature to oxygen diffusion (Harris and Vogeli, 2010; King and Valley, 2001; Lackey et al., 2006, 2008, 2011, 2012). The $\delta^{18}O$ values of Khajeh Morad aplite and pegmatite garnets (~10.3‰) are similar to magmatic garnets measured globally (e.g. 6.12–7.27‰, Harangi et al., 2001; 7.3–11.6‰, Vielzeuf et al., 2005; 10–11.4‰, Harris and Vogeli, 2010; 7.5–8.2‰, Lackey et al., 2011; Fig. 13, Table 6) and lower than metamorphic garnet (e.g. ~11.4 to 13.4‰, Kohn et al., 1997; Stevens et al., 2007). The $\delta^{18}O$ values of garnet in Khajeh Morad aplite and pegmatite garnet are similarly lower than those values for garnets from local metamorphic complex (e.g. schists from Dehnow and Khalaj areas in the northwest and

Table 6
Some chemical characteristics of magmatic, metapelitic and aplite–pegmatite garnets.

Garnet origin	Magmatic garnets in granitoids[1]	Magmatic garnets in granitic aplite–pegmatite[2]	Metamorphic garnets in metapelites[1]
Metamorphic mineral inclusion in garnet	No	No	Yes
Chemical composition	alm–grs	alm–sps	alm–sps
$Mg\#^{3}_{garnet/whole\ rock}$	~0.31	~0.14	~0.16
$(Mg/Fe)^{Grt}(Mg/Fe)Bt^{4}$	>~0.24	>~0.24	<~0.20
CaO and MnO of garnet	CaO > MnO	CaO < MnO	CaO < MnO
alm, grs, prp, sps in garnet	alm > grs > prp > sps	alm > sps > prp > grs	alm > sps > prp > grs
alm zoning (core-to-rim) in garnet	−	+	+
sps zoning (core-to-rim) in garnet	+	−	−
grs zoning (core-to-rim) in garnet	−	+	−
prp zoning (core-to-rim) in garnet	+	+	+
HREE/Chondrite ratio in garnet[5]	~1000	~1000	~100
$\delta^{18}O$ of garnet[6]	<~11.6‰	<~10.3‰	>~11.4‰

Note: decrease (−), increase (+); 1: data of magmatic garnet in granitoid and metamorphic garnets in schists are from Samadi et al. (2014b) and references therein; 2: data from Khajeh Morad, Baldwin and Von Knorring (1983), Manning (1983), Whitworth (1992), Macleod (1992), Thöni et al. (2003), Thöni and Miller (2004), Muller et al. (2012), and Gadas et al. (2013); 3: data from Samadi (2014); 4: Lyons and Morse (1970); 5: data of magmatic garnet in granitoid from Harangi et al. (2001) and data of metamorphic garnets in schists from El Korh et al. (2009); 6: data from Table 5 and references in Fig. 13.

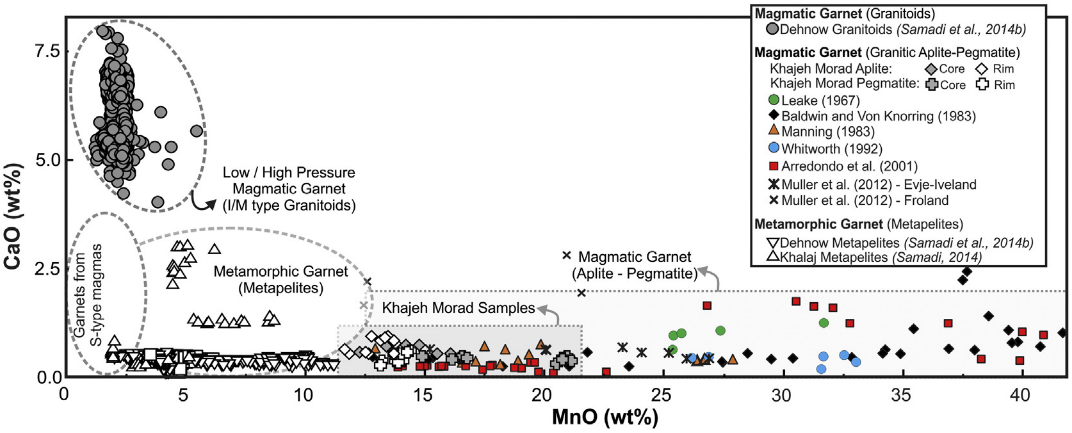

Fig. 7. Comparison of CaO versus MnO contents (wt.%) of garnets in Khajeh Morad granitic aplite–pegmatite with magmatic and metamorphic garnets from granitoids and metapelitic rocks of Dehnow and Khalaj areas (Samadi, 2014; Samadi et al., 2014b), magmatic garnet from granitic aplite–pegmatites of Leake (1967), Baldwin and Von Knorring (1983), Manning (1983), Whitworth (1992), Arredondo et al. (2001), and Muller et al. (2012) on the modified diagram of Harangi et al. (2001) (for interpretation of the references to color in this figure legend, the reader is referred to the web version of the article).

south of Mashhad) which have $\delta^{18}O$ values ranging from 13.0 to 12.7‰ (Table 5; Samadi et al., 2014b; Samadi, 2014). Applying the fractionation equation of Valley et al. (2003) yields temperatures of 625 °C and 628 °C (for aplite and pegmatite, respectively) which are much lower than the closure temperature of oxygen diffusion for garnet (>800 °C, Farquhar et al., 1996). In fact, diffusion of oxygen would have continued in quartz to lower temperature than in garnet. Depending on what other minerals were present, the quartz $\delta^{18}O$ value would have increased and the garnet $\delta^{18}O$ stayed the same, thus giving larger $\Delta_{\text{quartz–garnet}}$ and lower temperature. We interpret the garnet $\delta^{18}O$ values of Khajeh Morad aplite and pegmatite to be controlled by the melt composition, and to be unaffected by the subsequent involvement of external fluids or by metamorphism.

5.4. Genesis of garnet

The large negative Eu anomalies (Eu/Eu* < 0.1) of studied garnet grains are consistent with their growth from granitic melt. Low oxygen fugacity as well as simultaneous and/or primary crystallization of feldspar before garnet may account negative Eu (and Sr) anomalies of garnets.

However, the absence of garnet in the host granitoid rocks, together with the high Mn content of garnet in Khajeh-Morad aplite and pegmatite ($\text{sps}_{\text{aplite}}$: ~29–37 mole%; $\text{sps}_{\text{pegmatite}}$: ~30–50 mole%), implies that these garnets cannot be a residual refractory phase following anatexis, nor can they be products of partial melting from a garnet-bearing host rock. The Khajeh Morad garnets also exhibit core-to-rim decrease in Y, HREE, and Mn. Several scenarios promoting REE dissolution and diffusion rates in garnet while degreasing $\text{REE}_{\text{garnet/melt}}$ may account for these observations, including: (1) an increase in pressure during crystallization, (2) changes in residual melt composition accompanying garnet (or other mineral) crystallization, whereby Y, HREE and Mn are scavenged from the melt, and/or (3) an increase in the fluid content of late stage melts.

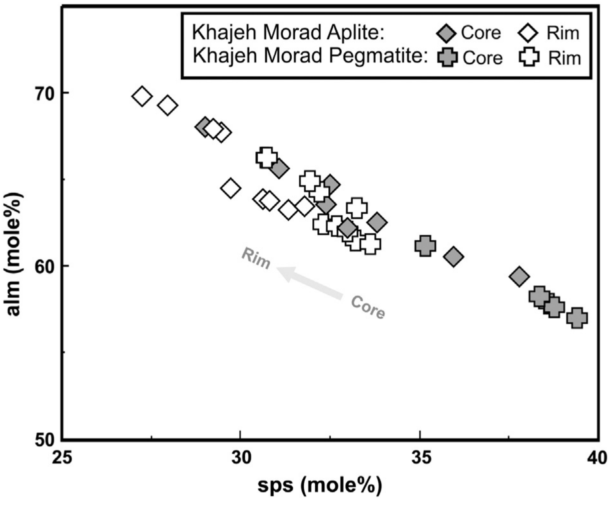

Fig. 8. Plot of sps versus alm contents (mole%) of rim and core of garnets in the Khajeh Morad aplite–pegmatite veins.

The occurrence of Mn-rich garnets in aplite and pegmatite veins could instead result from garnet neo-crystallization from a low-pressure (<5 kbar) fractionated melt during late stage magmatism (Manning, 1983). Apart from garnet, no other minerals (e.g. quartz, feldspar, and muscovite) in the Khajeh-Morad aplite and pegmatite tolerate or otherwise retain appreciable amounts of Y, HREE, and Mn. Thus, we suggest that the observed core-to-rim decrease in Y and HREE in aplite- and pegmatite-associated garnets reflects the evolving H_2O content of the melt, which caused REE dissolution, whereas core-to-rim decrease of Mn reflects changing melt composition as garnets crystallized and scavenged Mn.

5.5. Genesis of aplite–pegmatite

It is well accepted that most pegmatites originate from residual melts derived from the crystallization of granitic magmas, but some pegmatites may also form by protracted fractional crystallization and anatexis of rocks (Simmons and Webber, 2008). On the basis of geochemical finger printing, Thomas and Davidson (2013) show that a large proportion of granitic pegmatites could be genetically related to a main granite body. In the Mashhad granitoid batholith, aplite and pegmatite veins occur within granodiorite and monzogranite. According to Samadi et al. (2014a) and Samadi (2014), the Mashhad granodiorite is a mantle-derived I-type suite, whereas the younger magmatic phase of monzogranite is a strongly peraluminous S-type granite formed by dehydration-melting of heterogeneous metasedimentary assemblages in a thickened lower continental crust. The core-to-rim major element variations of garnets in Khajeh Morad pegmatite veins are similar to magmatic garnets of REE-Li pegmatites from Steli (Evje-Iveland, southern Norway, Muller et al., 2012), which have compositional affinities to S-type granites (Chappell and White, 2001) of crustal origin (Cerný et al., 2012). The $\delta^{18}O$ values of the garnet and quartz can also help trace the origin of pegmatite-forming melts. Assuming a $\Delta_{\text{quartz–magma}}$ value of 1.1‰, as suggested by Fourie and Harris (2011), the original

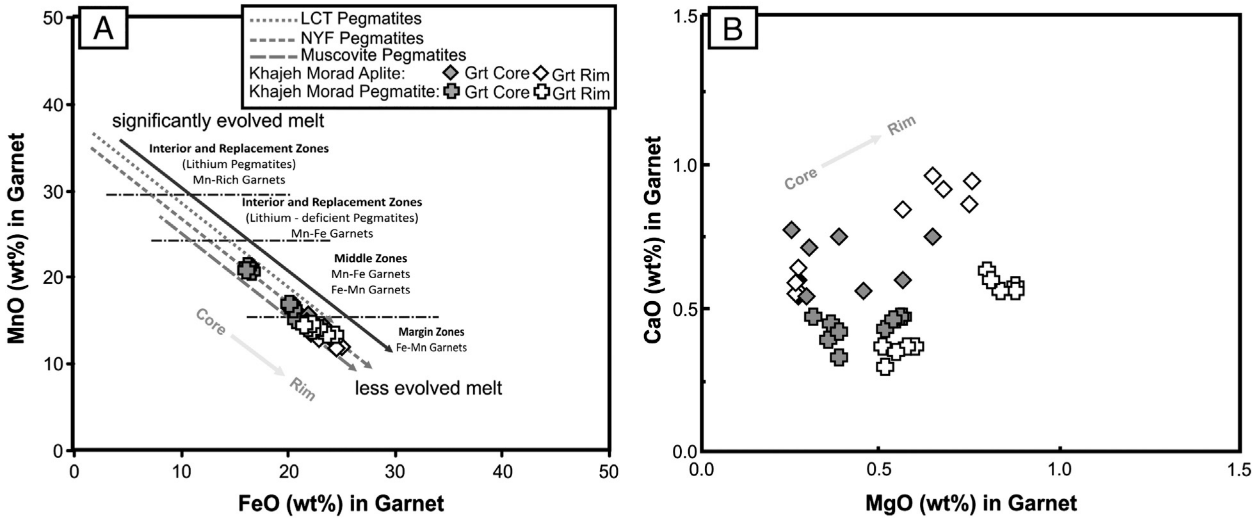

Fig. 9. Garnets from Khajeh Morad aplite–pegmatite veins on: (A) FeO versus MnO (wt.%) plot (based on data of Moretz et al. (2013) and references therein); (B) MgO versus CaO (wt.%) plot.

Khajeh Morad aplite and pegmatite magmas had $\delta^{18}O$ values averaging 12.6‰ and 12.5‰, respectively (Table 5). Alternatively, if the garnet is assumed to crystallize at 750 °C, the value of $\Delta_{quartz–garnet}$ determined using the equation of Valley et al. (2003) can be combined with the value of 0.4 for $\Delta_{quartz–magma}$ of Bindeman et al. (2008) to give a value of $\Delta_{garnet\text{-}magma}$ of 2.19‰. If combined with the average garnet value of

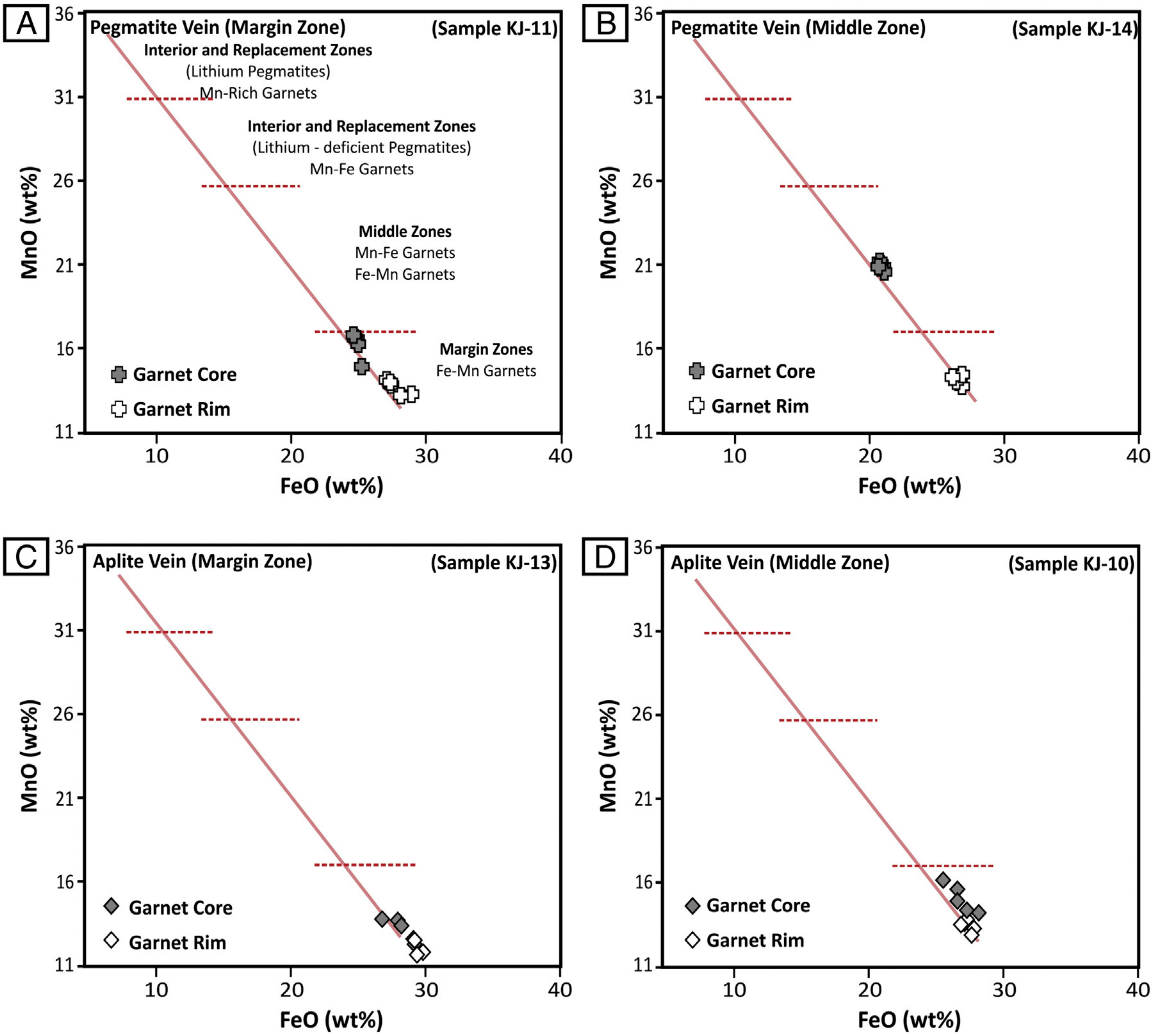

Fig. 10. Relationship between the chemical composition of garnet and pegmatite zones (Baldwin and Von Knorring, 1983). Chemical variation of magmatic garnet core and rim in: (A) the margin zone of pegmatite vein; (B) the middle zone of pegmatite vein; (C) the margin zone of aplite vein; (D) the middle zone of aplite vein.

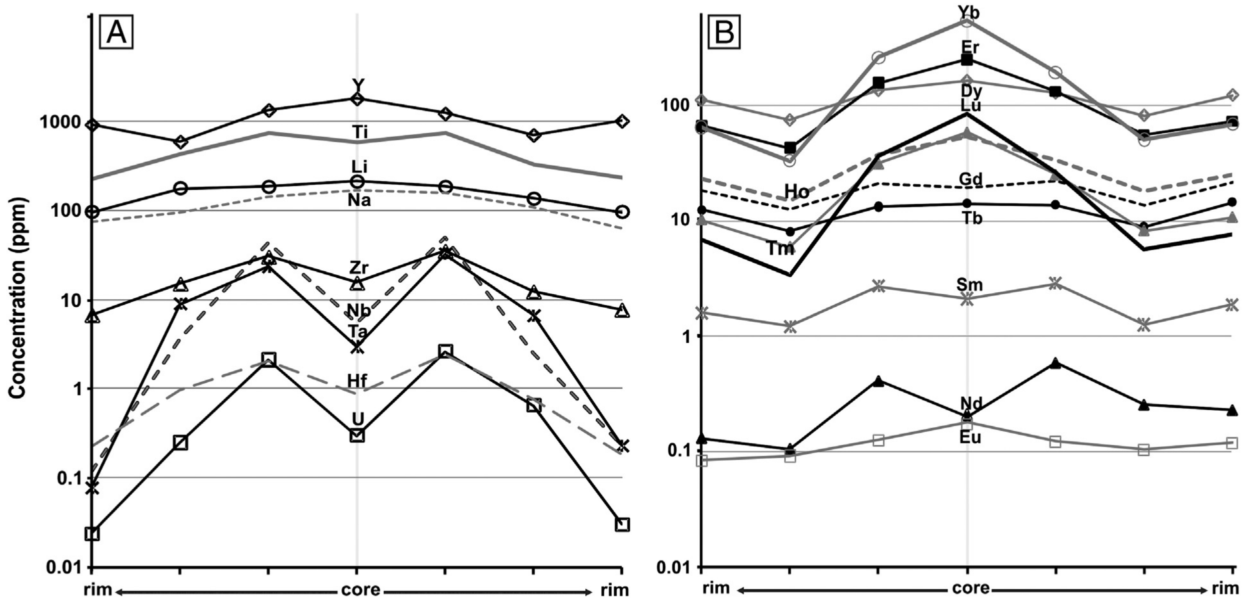

Fig. 11. Element concentrations in a transection of a coarse garnet grain (rim-core-rim profile) in aplite.

10.3‰ for the samples, this suggests a magma δ^{18}O value of 12.5‰. The two estimates of magma δ^{18}O value agree well, and are within the compositional ranges of S-type granitoid magmas (e.g. Cape Granite suite, Harris et al., 1997; Felahiyei and Dananciobasi granitoids, Boztuğ and Arehart, 2007), but higher than δ^{18}O values of I-type granitoid magmas (e.g. Cape Yozgat batholith and Konur granitoids, Boztuğ and Arehart, 2007; Beypazari granitoid, Öztürk et al., 2012; Dehnow granitoid, Samadi et al., 2014b). We therefore suggest that our δ^{18}O values of quartz and garnet in the Khajeh Morad aplite and pegmatite point to the derivation of these aplite and pegmatite from parental melts of S-type monzogranite rather than I-type granodiorite. In addition, the lower δ^{18}O values (<~10.3‰, Table 6) of garnet in Khajeh Morad aplite and pegmatite are consistent with the idea that garnet is a magmatic phase that crystallized from a fractionated melt, and further supported by core-to-rim decreases in Y and REE for garnet (Muller et al., 2012; Smeds, 1994) (Figs. 11 and 12). The appearance of Mn-rich garnet during fractional crystallization is likely related to strong partitioning of Mn^{2+} into the liquid relative to muscovite or biotite (Abbott, 1985). Higher CaO and TiO_2 of garnet in aplite (Tables 3 and 4), compared to pegmatite, may indicate differentiation from comparatively more primitive granitic magma.

Petrologists typically choose a liquidus temperature between 650 °C and 750 °C as the temperature of the pegmatite-forming melt upon emplacement (London, 2014). According to London (2014), some mineralogical thermometers that are usable in granites and rhyolites are not feasible for pegmatites (e.g. zircon saturation temperatures, Fe–Ti oxide thermometers, Ti-in-quartz thermometer). Here we suggest that the ternary feldspar system and oxygen isotope exchange thermometry may provide most reliable mineral thermometers. The minimum temperatures of aplite and pegmatite melts, using two-feldspar thermometry (Haselton et al., 1983) are 572 °C (for aplite) and 620 °C (for pegmatite). Application of the Ternary feldspar P-T calculation by SOLVCALC (Wen and Nekvasil, 1994; using Margules fitting parameters of Elkins and Grove, 1990) indicates vein emplacement temperatures of

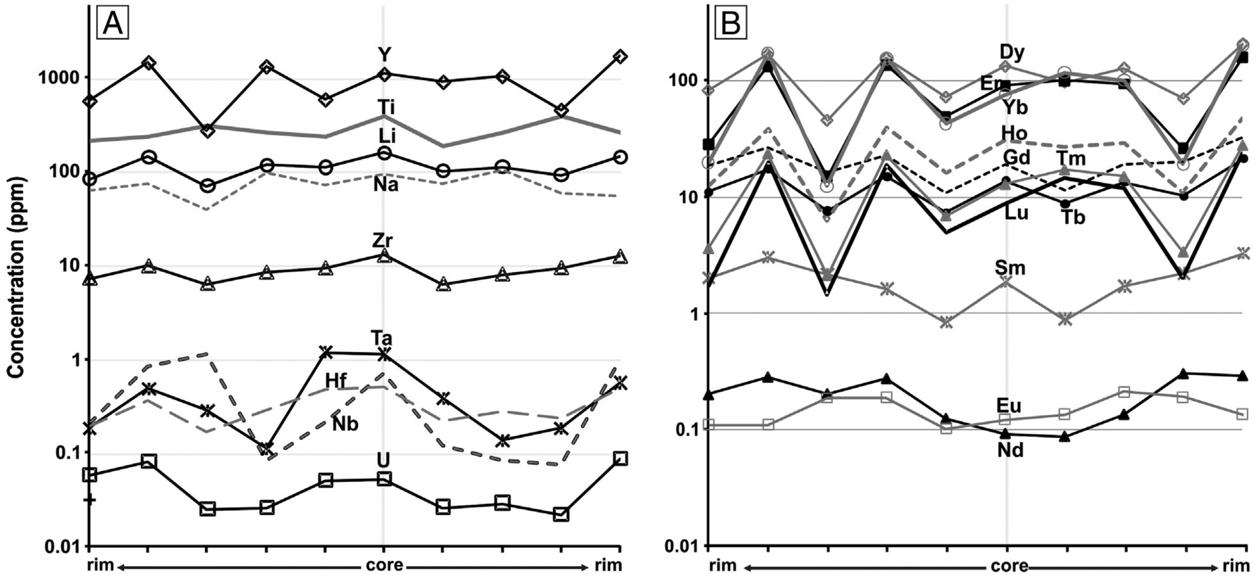

Fig. 12. Element concentrations in a transection of a coarse garnet grain (rim-core-rim profile) in pegmatite.

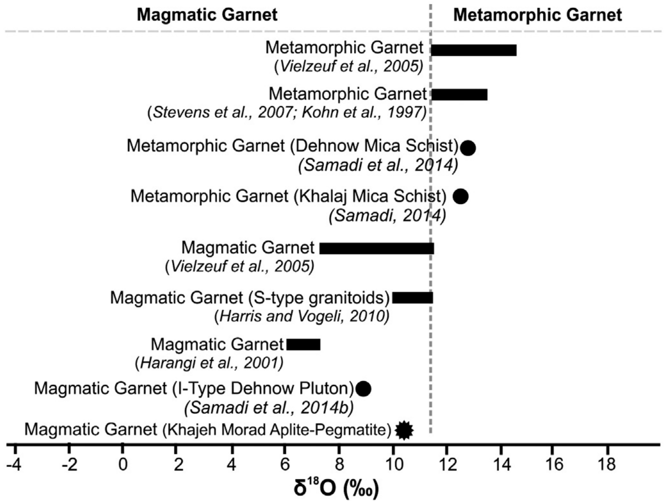

Fig. 13. Comparison of $\delta^{18}O$ values in magmatic garnet in aplite–pegmatite with magmatic and metamorphic garnets in granitoids and metamorphic rocks.

340 °C for aplite and 440 °C for pegmatite. These binary and tertiary feldspar temperatures are substantially lower than closure temperatures indicated for oxygen isotope exchange between garnet and quartz pairs (i.e. 625 °C and 628 °C, Table 5) after garnet crystallization.

Following crystallization of the aplite veins, an increased fluid flux to the residual melts could have lowered crystallization temperatures, nucleation rates, melt polymerization and viscosity, leading to increased diffusion rates and solubility (Simmons and Webber, 2008). We suggest that all of these factors led to the development of coarse crystals in the pegmatite veins.

6. Conclusions

Garnets from aplite and pegmatite of Khajeh Morad in the vicinity of Mashhad City, in northeastern Iran, are magmatic in origin. They have MnO >12 wt.% and CaO <~2 wt.% and show normal zoning with core-to-rim decrease in Mn and core-to-rim increase in Fe, Mg, and Ca, similar to metamorphic and xenocrystic garnets in common granitoids. Mn and Fe in garnet support a low degree of melt evolution for aplite associations, and a higher (low-to-moderate) degree of melt evolution for pegmatite associations. The core-to-rim decrease of MnO/(FeO + MnO) of garnet crystals may be caused by (1) Mn-scavenging during garnet crystallization and consequent depletion in the residual melts, as garnets are the main Mn consuming phase in the aplite–pegmatite forming melts, in addition to (2) H_2O activity in magma during the pegmatite crystallization.

The REEs, Y, Zr, Nb, Ta, Hf and U show core-enrichments in aplite garnet but have irregular core-to-rim distributions in pegmatite garnet. We speculate that the fluid content of the magma, which acts to promote REE dissolution and diffusion rates and decrease $REE_{garnet/melt}$, was likely responsible for the rim-margin decreases in Y and REE observed in Khajeh Morad garnets. The $\delta^{18}O$ values of garnets from Khajeh Morad aplite and pegmatite, along with those for associated quartz, support that these phases crystallized from a fractionated S-type melt.

Acknowledgements

We thank the Science and Research Branch, the University of Texas at Austin, the University of Cape Town, the NRF (South Africa), and Institute for Research on Earth Evolution (Yokosuka, Japan) for financial supports and access to geochemical facilities. The authors express gratitude to the constructive reviews of Richard N. Abbot, and one anonymous reviewer and the editorial handling of associated editor Nelson Eby, which improved the original article.

References

Abbott Jr., R.N., 1981a. The role of manganese in the paragenesis of magmatic garnet: an example from the Old Woman-Piute Range, California: a discussion. The Journal of Geology 89, 767–769.

Abbott Jr., R.N., 1981b. AFM liquidus projection for granitic magmas, with special reference to hornblende, biotite and garnet. The Canadian Mineralogist 19, 103–110.

Abbott Jr., R.N., 1985. Muscovite bearing granites in the AFM liquidus projection. The Canadian Mineralogist 23, 553–561.

Alavi, M., 1991. Sedimentary and structural characteristics of the Paleo-Tethys remnants in northeastern Iran. Geological Society of America Bulletin 103 (8), 983–992.

Allan, B.D., Clarke, D.B., 1981. Occurrence and origin of garnets in the south mountain batholith, Nova Scotia. The Canadian Mineralogist 19, 19–24.

Arredondo, E.H., Rossman, G.R., Lumpkin, G.R., 2001. Hydrogen in spessartine–almandine garnets as a tracer of granitic pegmatite evolution. American Mineralogist 86, 485–490.

Aydar, E., Gourgaud, A., 2002. Garnet-bearing basalts: an example from Mt. Hasan, Central Anatolia, Turkey. Mineralogy and Petrology 75, 185–201.

Baldwin, J.R., Von Knorring, O., 1983. Compositional range of Mn-garnet in zoned granitic pegmatites. The Canadian Mineralogist 21, 683–688.

Bindeman, I.N., Fu, B., Kita, N.T., Valley, J.W., 2008. Origin and evolution of silicic magmatism at Yellowstone based on ion microprobe analysis of isotopically zoned zircons. Journal of Petrology 49, 163–193.

Boztuğ, D., Arehart, G.B., 2007. Oxygen and sulfur isotope geochemistry revealing a significant crustal signature in the genesis of the post-collisional granitoids in central Anatolia, Turkey. Journal of Asian Earth Sciences 30, 403–416.

Cerný, P., London, D., Novák, M., 2012. Granitic Pegmatites as Reflections of Their Sources. Elements 8, 289–294.

Chappell, B.W., White, A.J.R., 2001. Two contrasting granite types, 25 years later. Australian Journal of Earth Sciences 48, 489–499.

Čopjaková, R., Sulovský, P., Paterson, B.A., 2005. Major and trace elements in pyrope-almandine garnets as sediment provenance indicators of the lower carboniferous culm sediments, Drahany uplands, Bohemian Massif. Lithos 82, 51–70.

Dahlquist, J.A., Galindo, C., Pankhurst, R.J., Rapela, C.W., Alasino, P.H., 2007. Magmatic evolution of the Peñón Rosado granite: petrogenesis of garnet-bearing granitoids. Lithos 95, 177–207.

Day, R.A., Green, T.H., Smith, I.E.M., 1992. The origin and significance of garnet phenocrysts and garnet-bearing xenoliths in Miocene calc-alkaline volcanics from Northland, New Zealand. Journal of Petrology 33, 125–161.

Deer, W.A., Howie, R.A., Zussman, J., 1982. Rock-Forming Minerals, Volume IA, Orthosilicates. Longman, New York.

Deer, W.A., Howie, R.A., Zussman, J., 1992. An introduction to the rock-forming minerals, 2nd edition. Longmans, London.

El Korh, A., Schmidt, S.T., Ulianov, A., Potel, S., 2009. Trace element partitioning in HP–LT metamorphic assemblages during subduction-related metamorphism, Ile de Groix, France: a detailed LA-ICPMS study. Petrology 50 (6), 1107–1148.

Elkins, L.T., Grove, T.L., 1990. Ternary feldspar experiments and thermodynamic models. American Mineralogist 75, 544–559.

Farquhar, J., Chacko, T., Ellis, D.J., 1996. Preservation of oxygen isotope compositions in granulites from Northwestern Canada and Enderby Land, Antarctica: implications for high-temperature isotopic thermometry. Contributions to Mineralogy and Petrology 125, 213–224.

Fourie, D.S., Harris, C., 2011. O-isotope study of the Bushveld Complex granites and granophyres: constraints on source composition, and assimilation. Journal of Petrology 152, 2221–2242.

Gadas, P., Novák, M., Talla, D., Galiová, M.V., 2013. Compositional evolution of grossular garnet from leucotonalitic pegmatite at Ruda nad Moravou, Czech Republic; a complex EMPA, LA-ICP-MS, IR and CL study. Mineralogy and Petrology 107, 311–326.

Green, D.H., Ringwood, A.E., 1968. Origin of the garnet phenocrysts in calc-alkaline rocks. Contributions to Mineralogy and Petrology 18, 163–174.

Harangi, S.Z., Downes, H., Ko´sa, L., Szabo´, C.S., Thirlwall, M.F., Mason, P.R.D., 2001. Almandine garnet in calc-alkaline volcanic rocks of the Northern Pannonian Basin (Eastern-Central Europe): geochemistry, petrogenesis and geodynamic implications. Journal of Petrology 42, 1813–1843.

Harris, C., Ashwal, L.D., 2002. The origin of low $\delta^{18}O$ granites and related rocks from the Seychelles. Contributions to Mineralogy and Petrology 143, 366–376.

Harris, C., Vogeli, J., 2010. Oxygen isotope composition of garnet in the Peninsula Granite, Cape Granite Suite, South Africa: constraints on melting and emplacement mechanisms. South African Journal of Geology 113 (4), 401–412.

Harris, C., Faure, K., Diamond, R.E., Scheepers, R., 1997. Oxygen and hydrogen isotope geochemistry of S and I-type granitoids: the Cape Granite suite, South Africa. Chemical Geology 143, 95–114.

Harrison, T.N., 1988. Magmatic garnets in the Cairngorm granite, Scotland. Mineralogical Magazine 52, 659–667.

Haselton, H.T., Hovis, G.L., Hemingway, B.S., Robie, R.A., 1983. Calorimetric investigation of the excess entropy of mixing in albite - sanidine solid solution; lack of evidence for Na, K short range order and implication for two feldspars thermometry. American Mineralogist 68, 398–413.

Heimann, A., Spry, P.G., Teale, G.S., Conor, C.H.H., Pearson, N.J., 2011. The composition of garnet in garnet-rich rocks in the southern Proterozoic Curnamona Province, Australia: an indicator of the premetamorphic physicochemical conditions of formation. Mineralogy and Petrology 101, 49–74.

Hellstrom, J., Paton, C., Woodhead, J., Hergt, J., 2008. Iolite: software for spatially resolved LA-(quad and MC) ICPMS analysis. Mineralogical Association of Canada Short Course series 40, pp. 343–348.

Irving, A.J., Frey, F.A., 1978. Distribution of trace-elements between garnet megacrysts and host volcanic liquids of Kimberlite to Rhyolitic composition. Geochimica et Cosmochimica Acta 42, 771–787.

Jaffe, H.W., 1951. The role of yttrium and other minor elements in the garnet group. American Mineralogist 36, 133–155.

Kano, H., 1983. On the origin of garnets in the Setouchi andesites. Scientific and Technical Report of Mining College 4. Akita University, pp. 41–46.

Kawabata, H., Takafuji, N., 2005. Origin of garnet crystals in calcalkaline volcanic rocks from the Setouchi volcanic belt, Japan. Mineralogical Magazine 69, 951–971.

King, E.M., Valley, J.W., 2001. The source, magmatic contamination, and alteration of the Idaho Batholith. Contributions to Mineralogy and Petrology 142, 72–88.

Koepke, J., Falkenberg, G., Rickers, K., Diedrich, O., 2003. Trace element diffusion and element partitioning between garnet and andesite melt using synchrotron X-ray fluorescence microanalysis (μ-SRXR). European Journal of Mineralogy 15 (1), 883–892.

Kohn, M.J., Spear, F.S., Valley, J.W., 1997. Dehydration melting and fluid recycling during metamorphism: Rangeley Formation, New Hampshire, USA. Journal of Petrology 38, 1255–1277.

Kontak, D.J., Kyser, T.K., 2009. Nature and origin of an LCT-suite pegmatite with late-stage sodium enrichment, Brazil Lake, Yarmouth County, Nova Scotia. II. Implications of stable isotopes (δ^{18}O, δD) for magma source, internal crystallization and nature of sodium metasomatism. The Canadian Mineralogist 47, 745–764.

Kretz, R., 1983. Symbols for rock forming minerals. American Mineralogist 68 (1/2), 277–279.

Lackey, J.S., Valley, J.W., Hinke, H.J., 2006. Deciphering the source and contamination history of peraluminous magmas using δ^{18}O of accessory minerals: examples from garnet-bearing plutons of the Sierra Nevada batholiths. Contributions to Mineralogy and Petrology 151, 20–44.

Lackey, J.S., Valley, J.W., Chen, J.H., Stockli, D.F., 2008. Dynamic magma systems, crustal recycling, and alteration in the Central Sierra Nevada Batholith: the oxygen isotope record. Journal of Petrology 49 (7), 1397–1426.

Lackey, J.S., Erdmann, S., Hark, J.S., Nowak, R.M., Murray, K.E., Clarke, D.B., Valley, J.W., 2011. Tracing garnet origins in granitoid rocks by oxygen isotope analysis: examples from the South Mountain batholith, Nova Scotia. The Canadian Mineralogist 49, 417–739.

Lackey, J.S., Romero, G.A., Bouvier, A.S., Valley, J.W., 2012. Dynamic growth of garnet in granitic magmas. Geology 40, 171–174.

Leake, B.E., 1967. Zoned garnets from the Galway granite and its aplite. Earth and Planetary Science Letters 3, 311–315.

London, D., 2008. Pegmatites. The Canadian MineralogistSpecial Publication 10.

London, D., 2014. A petrologic assessment of internal zonation in granitic pegmatites. Lithos 184–187, 74–104.

Lyons, J.B., Morse, S.A., 1970. Mg/Fe partitioning in garnet and biotite from some granitic, pelitic, and calcic rocks. American Mineralogist 55, 231–245.

Macleod, G., 1992. Zoned manganiferous garnets of magmatic origin from the Southern Uplands of Scotland. Mineralogical Magazine 56, 115–116.

Manning, D.A.C., 1983. Chemical variation in garnets from aplites and pegmatites, peninsular Thailand. Mineralogical Magazine 47, 353–358.

McDonough, W.F., Sun, S.S., 1995. The composition of the Earth. Chemical Geology 120, 223–253.

Miller, C.F., Stoddard, E.F., 1981a. The role of manganese in the paragenesis of magmatic garnet: an example from the Old Woman Piute Range, California. The Journal of Geology 89, 233–246.

Miller, C.F., Stoddard, E.F., 1981b. The role of manganese in the paragenesis of magmatic garnet: an example from the Old Woman Piute Range, California: a reply. The Journal of Geology 89, 233–246.

Mirnejad, H., Blourian, G.H., Kheirkhah, M., Akrami, M.A., Tutti, F., 2008. Garnet-bearing rhyolite from Deh-Salm area, Lut block, Eastern Iran: anatexis of deep crustal rocks. Mineralogy and Petrology 94, 259–269.

Mirnejad, H., Lalonde, A.E., Obeid, M., Hassanzadeh, J., 2013. Geochemistry and petrogenesis of Mashhad granitoids: an insight into the geodynamic history of the Paleo-Tethys in Northeast of Iran. Lithos 170–171, 105–116.

Moretz, L., Heimann, A., Bitner, J., Wise, M., Rodrigues Soares, D., Mousinho Ferreira, A., 2013. The composition of garnet as indicator of rare metal (Li) mineralization in granitic pegmatites. Proceeding of The 6th International Symposium on Granitic Pegmatites, pp. 94–95.

Muller, A., Kearsley, A., Spratt, J., Seltmann, R., 2012. Petrogenetic implications of magmatic garnet in granitic pegmatites from southern Norway. The Canadian Mineralogist 50, 1095–1115.

Natalin, B.A., Sengor, A.M.C., 2005. Late Paleozoic to Triassic evolution of the Turan and Scythian platforms: the pre-history of the Palaeo-Tethyan closure. Tectonophysics 404, 175–202.

Öztürk, Y.Y., Helvaci, C., Satir, M., 2012. Geochemical and isotopic constraints on petrogenesis of the Beypazarı granitoid, NW Ankara, Western Central Anatolia, Turkey. Turkish Journal of Earth Sciences 21, 53–77.

Patranabis-Deb, A., Schieber, J., Basu, A., 2008. Almandine garnet phenocrysts in a 1Ga rhyolitic tuff from Central India. Geological Magazine 1–11.

Samadi, R., 2009. The origin of garnet megacrysts from Dehnow Tonalite, Northwest of Mashhad(M.Sc. thesis) Department of Geology, Faculty of Sciences, University of Tehran, Tehran, Iran (179 pp.).

Samadi, R., 2014. Chemistry and origin of garnet in the granitoids and metamorphic rocks in the south of Mashhad (Khajeh Morad, Khalaj and Dehnow)(Ph.D. thesis) Department of Geology, Science and Research Branch, Islamic Azad University, Tehran, Iran (364 pp.).

Samadi, R., Valizadeh, M.V., Mirnejad, H., Kawabata, H., 2012. Geothermometry and geobarometry of metamorphic rocks of Dehnow (Northwest of Mashhad). Journal of Geosciences 21 (84), 3–14.

Samadi, R., Gazel, E., Mirnejad, H., Kawabata, H., Baharifar, A.A., Sheikh-Zakaraiee, S.J., 2014a. Paleo-Tethys subduction in the center of the Alpine-Himalayan orogenic system in the Triassic: evidence from geochemistry of I-type granitoids from Dehnow pluton, NE Iran. Neues Jahrbuch für Geologie und Paläontologie (Abhandlungen) 271 (3), 285–306.

Samadi, R., Mirnejad, H., Kawabata, H., Valizadeh, M.V., Harris, C., Gazel, E., 2014b. Magmatic garnet in the Triassic (215 Ma) Dehnow pluton of NE Iran and its petrogenetic significance. International Geology Review 56 (5), 596–621.

Schwandt, C.S., Papike, J.J., Shearer, C.K., 1996. Trace element zoning in pelitic garnet of the Black Hills, South Dakota. American Mineralogist 81, 1195–1207.

Simmons, W.B., Webber, K.L., 2008. Pegmatite genesis: state of the art. European Journal of Mineralogy 20, 421–438.

Smeds, S.A., 1994. Zoning and fractionation trends of a peraluminous NYF pegmatite field at Falun, south-central Sweden. GFF 116, 175–184.

Smith, M.P., Henderson, P., Jeffries, T.E.R., Long, J., Williams, C.T., 2004. The rare earth elements and uranium in garnets from the Beinn an Dubhaich Aureole, Skye, Scotland, UK: constraints on processes in a dynamic hydrothermal system. Journal of Petrology 45 (3), 457–484.

Spear, F.S., Kohn, M.J., 1996. Trace element zoning in garnet as a monitor of crustal melting. Geology 24 (12), 1099–1102.

Stevens, G., Villaros, A., Moyen, J.F., 2007. Selective peritectic garnet entrainment as the origin of geochemical diversity in S-type granites. Geology 35, 9–12.

Thomas, R., Davidson, P., 2012. Water in granite and pegmatite-forming melts. Ore Geology Reviews 46, 32–46.

Thomas, R., Davidson, P., 2013. The missing link between granites and granitic pegmatites. Journal of Geosciences 58, 183–200.

Thöni, M., Miller, C., 2004. Ordovician meta-pegmatite garnet (NW Ötztal basement, Tyrol, Eastern Alps): preservation of magmatic garnet chemistry and Sm-Nd age during mylonitization. Chemical Geology 209, 1–26.

Thöni, M., Petrík, I., Janák, M., Lupták, B., 2003. Preservation of Variscan garnet in Alpine metamorphosed pegmatite from the Veporic Unit, Western Carpathians: evidence from Mm–Nd isotope data. Journal of the Czech Geological Society 48 (1–2), 123–124.

Valley, J.W., Bindeman, I.N., Peck, W.H., 2003. Empirical calibration of oxygen isotope fractionations in zircon. Geochimica et Cosmochimica Acta 67 (17), 3257–3266.

Vielzeuf, D., Veschambre, M., Brunet, F., 2005. Oxygen isotope heterogeneities and diffusion profile in composite metamorphic-magmatic garnets from the Pyrenees. American Mineralogist 90, 463–472.

Wang, R., Hu, H., Zhang, A., Xu, S., Wang, D., 2003. Yttrium zoning in garnet from the Xihuashan granitic complex and its petrological implications. Chinese Science Bulletin 48, 1611–1615.

Wen, S., Nekvasil, H., 1994. SOLVCALC: an interactive graphics program package for calculating the ternary feldspar solvus and for two-feldspar geothermometry. Computers and Geosciences 20 (6), 1025–1040.

Whitney, D.L., Evans, B.W., 2010. Abbreviations for names of rock-forming minerals. American Mineralogist 95, 185–187.

Whitworth, M.P., 1992. Petrogenetic implications of garnets associated with lithium pegmatites from SE Ireland. Mineralogical Magazine 56, 75–83.